1

Introduction

The development of Deep Neural Networks (DNNs) made tasks such as object classification [26] and object detection [40], [17] easy to solve. These DNNs has been deployed in various real world scenarios such as autonomous driving [29], semi-autonomous robotic surgery [34] and also in space rovers [31], [4]. DNNs are majorly deployed in the perception stack in the autonomous driving pipeline. Figure 1.1 depicts the pipeline of the modules present in one of the open source autonomous driving platform called Apollo [12]. From this pipeline, one can infer that the most of the decisions regarding the vehicle control made by autonomous system is dependent on the output of the perception module. Since the perception module plays such significance, the developers of the perception stack must make sure the outputs are meaningful.

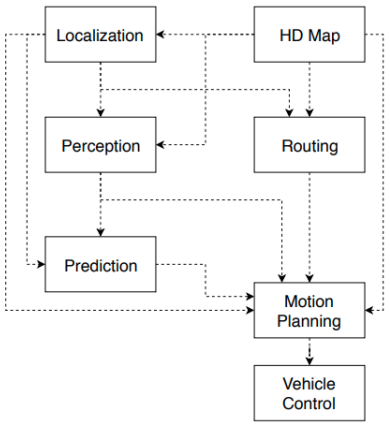

Figure 1.1: Module pipeline for Apollo autonomous driving platform. Image taken from [12]

The DNNs utilized in perception module need to be trained on the dataset which should be similar to area of its deployment. For example, an autonomous driving agent must be trained on dataset containing roads, vehicles, vegetation and other objects found around road. This closedness of the dataset i.e., fixed number of classes, will cause an issue when the DNN encounter an unknown object in real world. This unknown object is predicted as one of the class in the dataset, leading to radical decisions when this error is propogated down the pipeline in Figure 1.1. One such real world problem is encountered by the Tesla

autonomous driving platform.

(a) (b)

Figure 1.2: Misdetection of OOD objects in Tesla autonomous driving platform. (a) Moon is detected as yellow signal light and (b) depicts the misdetection of burger king sign as stop traffic sign. Images taken from [28]

Figure 1.2a and Figure 1.2b depicts the misdetections from the Tesla autonomous driving system. The problem in the first image, is the moon is detected as the yellow signal light and second image has the problem of misdetection of burger king sign as stop signal. These misdetections of unknown objects in the environment might lead to fatal consequences. This questions the safety of the Deep Neural Networks (DNNs) predictions and so an effort has been made in this thesis to detect these unknown objects in 3D LiDAR data using uncertainty score. The unknown obejcts in the real world which are not present in the training dataset can be regarded as out-of-distribution (OOD) objects. More discussion on the OOD is presented in Section 1.1.

1.1 OOD/Anomaly/Distributional shift

Let us time travel back to 18^{th} century and assume that we had implemented a DNN model to detect ships, the dataset images for training the DNN model will be similar to Figure 1.3a. 18^{th} century ships as in Figure 1.3a can be defined as "*ship contains hull and sails*". Fast forward to present time, current ships are as shown in Figure 1.3b. Ship as in 1.3b can be defined as "*ship contains hull and passenger decks stacked upon each other*". Now if we want to deploy the old model trained with old ships to detect the present generation of ships, it is diffcult because of the change in definition and properties of ship. This change in data distribution over a period of time is called "*distributional shift*" of the data.

Anomaly can be defined as the patterns that doesn't conform to the expected training behavior as proposed in [9]. By this definition, Figure 1.3c and Figure 1.3d can be considerd as anomalies. This is

(a) (b) (c)

(d) (e) (f)

Figure 1.3: Illustration of distributional shift, anomaly and out of distribution examples using various kind of ships. (a) represents the sail ship during 18th century. (b) depicts the current training data. (c), and (d) represents the anamolous ship data and (e), and (f) represents the OOD data. Images are taken from [46], [21], [33], [47], [14], and [54] respectively in the order they appear.

becuase Figure 1.3c is a container ship looking similar to Figure 1.3b instead of passenger decks we have containers stacked. Figure 1.3d is also anomaly because the Titanic also has a hull, passenger decks and chimneys. This additional chimnies as a fetures deviates this image from the definition of the ship and can be considered as "*anomaly*".

The input for out of distribution (OOD) is drawn from an unknown distribution of unknown data, which is not near to the trianing distribution. Figure 1.3e and Figure 1.3f are submarine and airship doesn't adhere to the definition of ship by any means. In general, one can argue that OOD can be defined as inputs which doesn't belong to any class in the training data. This kind of problem can also be called as Open Set Recognition (OSR) problem.

1.2 Problem Statement

In this thesis, we study the application of out-of-distribution (OOD) detection over the 3D semantic segmentation problem in the context of autonomous driving. Notably, we study the 3D semantic segmentation datasets available and create a benchmark for in-distribution and out-distribution for the OOD setting.

The other major issue, we address in this thesis is the OOD detection methods themselves. Existing OOD detection methods are developed on 2D classification and 2D semantic segmentation tasks and applicability of these methods on 3D semantic segmentation tasks is not studied. This is also challenging because the existing OOD methods are not easily adaptable to the 3D segmentation models because segmentation involves multi class classification and moreover high dimensionality of the 3D data impose

computational constraints.

The research questions answered by this thesis are:

R1 How to create a benchmark over 3D segmentation datasets for the OOD setting?, i.e., create the in-distribution and out-distribution datasets.

R2 How to extend current OOD detection methods from 2D classification task to 3D semantic segmentation?

R3 Is uncertainty quantification an effective approach to classify OOD detection in 3D semantic segmentation models?

R4 How to evaluate the OOD detections over the 3D semantic segmentation task?

1.2.1 Contributions

The contributions made in this thesis are

1. A complete survey on the available 3D LiDAR datasets
2. A detailed survey on existing 3D semantic segmentation models
3. Benchmarking of 3D LiDAR datasets for OOD detection. Proposed two benchmark datasets Sematic3D vs S3DIS and Semantic3D vs Toronto3D with Semantic3D being trianing dataset and S3DIS and Toronto3D being OOD datasets.
4. A survey on the uncertainty estimation methods and classical OOD methods.
5. An evaluation of OOD on benchmarked datasets over RandLA-Net model using Deep ensemble technique for uncertainty estimation.

To summarize this chapter, we discussed the motivation behind the problem of OOD detection like how errors in perception results lead to catastrophic consequences in an autonomous driving pipeline. Also discussed in detail about what an OOD and Anomaly are using a ship example and finally we discussed the contributions of this thesis. The following chapters include study of the state of the art, experimentation details and then followed by results and conclusion chapters.

2

State of the Art

In this chapter, we will discuss about the 3D LiDAR datasets available and made an attempt to classify them based on type of acquisition. Also we will discuss about the 3D semantic segmentation models, uncertainty estimation methods and OOD methods available.

2.1 3D LiDAR Datasets

LiDAR is one of the central component in the sensor suite for SLAM system in robotic applications [53], [37], [20] and autonomous driving [30]. 3D LiDAR data is preferred because, it can provide the exact replica of 3D geometry of the real world represented in the form of 3D point clouds. Because of these rich features and widespread use of LiDAR sensors, tasks such as 3D object detection [68], [66] and 3D semantic segmentation [39], [2] are becoming more predominant area for research.

In this section, we will discuss about the available 3D LiDAR datasets for 3D semantic segmentation task and classify the datasets based on acquisition methods as in [13]. [13] classifies the available public datasets into three classes based on the data acquisition process. They are *Sequential*, *Static* and *Synthetic* datasets. The data for sequential datasets are collected as frame sequences where mechanical LiDAR is mounted on top of a autonomous driivng platform as in Figure 2.1. Most of the popular autonomous

Figure 2.1: Sequential mounted LiDAR for data collection of Lyft L5 dataset. Image from [22]

driving datasets are of sequential type, but these kind of datasets comes with a drawback of sparse points than other datasets.

Static datasets consists of data collected from a stationary view point by a terrestrial laser scanner. These kind of datasets capture the static information of the realworld whereas the sequential datasets capture the dynamic movements of the surrounding objects. Static datasets find their way in applications such as the urban planning, augmented reality and robotics. Figure 2.2 depcits a terrestrial laser scanner

Figure 2.2: Terrestrial laser scanner in an industrial environment with the laser scanner mounted on a yellow tripod in the left corner of the floor. Image taken from [41]

used to capture point cloud of an industrial environment. An advantage with the static datasets, are they can produce highly dense point clouds leading to rich 3D geometric representations.

Last type of 3D LiDAR datasets are synthetic datasets. As the name suggests these datasets are generated from the computer simulation. Figure 2.3 depcits a simulated point cloud in a synthtic dataset called SynthCity. Eventhough synthetic datasets can be generated in large scale with cheap cost, they lack the accuracy in detail when compared to the point clouds generated from real world.

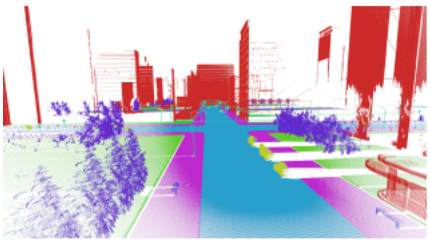

Figure 2.3: Illustration of a scene in synthetic dataset called SynthCity. Image taken from [18]

The datasets belonging to the each acquisition type are summed up in Table 2.1. Most of the datasets from the Table 2.1 are taken from [13] and also as a part of this study, additional new datasets were added to the list. The newly added datasets include DALES [57], ScanObjectNN [55] in static acquisition mode and AIO Drive [60], Toronto3D [49] are additions in the sequential mode. [13] also classifies GTAV **cite** dataset as synthetic 3D LiDAR but the corresponding paper doesn't report any LiDAR dataset and proposed only 2D dataset for segmentation. The limited number of datasets in 3D LiDAR allowed us to

study the characteristics of each individual datasets such as each class, data distribution and features of each point in point cloud. It is summarized in Table **ref** in Appendix **chapter number**

acquisition mode	dataset	frames	points (in million)	classes	scene type
static	Oakland[35]	17	1.6	44	outdoor
	Paris-lille-3D[43]	3	143	50	outdoor
	Paris-rue-Madame[45]	2	20	17	outdoor
	S3DIS[3]	5	215	12	indoor
	ScanObjectNN[55]	-	-	15	indoor
	Semantic3D[19]	30	4009	8	outdoor
	TerraMobilita/IQmulus[56]	10	12	15	outdoor
	TUM City Campus[15]	631	41	8	outdoor
	DALES[57]	40 (tiles)	492	8	outdoor
sequential	A2D2[16]	41277	1238	38	outdoor
	AIO Drive[60]	100	-	23	outdoor
	KITTI-360[64]	100K	18000	19	outdoor
	nuScenes-lidarseg[8]	40000	1400	32	outdoor
	PandaSet[63]	16000	1844	37	outdoor
	SemanticKITTI[5]	43552	4549	28	outdoor
	SemanticPOSS[36]	2988	216	14	outdoor
	Sydney Urban[11]	631	-	26	outdoor
	Toronto-3D[49]	4	78.3	8	outdoor
synthetic	SynthCity[18]	75000	367.9	9	outdoor

Table 2.1: 3D LiDAR datasets classified based on the acquisition type. Table updated from [13]

From the available datasets, we chose Semantic3D dataset as in-distribution (ID) training dataset. S3DIS is chosen as out-of-distribution (OOD) dataset as S3DIS is much different from Semantic3D. Detailed disussion on datasets were done in Chapter cite here.

2.2 3D semantic segmentation models

In this section, we will discuss about the methods available for 3D semantic segmentation. The discussion include a breif peek into traditional 3D semantic segmentation methods and study of deep learning based 3D point cloud segmentation.

Traditional methods involve a complex features extraction and pass these features to a classficiation algorithm such as Support Vector Machines or Random Forests to classify each point the point cloud. Various authors developed variety of methods to extract the features from the input point cloud. Some of these methods include segmentation from edge information [7], construction of complex graph pyramids [25]. 3D Hough transforms as in [58] and application of RANSAC [44] and [51]. These traditional methods are now outdated as DNNs proved to better at feature extraction.

2.2.1 Deep learning based 3D semantic segmentation

Deep learning based models are efficient at segmentation and can be divided into three types. Initial type include the point based models where the model directly feeds on the 3D point cloud. Then the

other type include projection based models where the model takes in a projected points into 2D image either a range image or bird's eye view. Final type of models include the use of graph neural networks. Point based models mostly utilize fully connected layer or convolutional layers. Where as the projection based models utilize existing 2D semantic segmentation archiecture. The detailed summary of each model belonging to these two categories are depicted in Table 2.2 along with number of parameters. Finally, graph neural networks are out of the scope for this project and will not be disucssed further.

Method	**Summary**	**Type**	**#Params**
PointNet[38]	PointNet works on raw point cloud and acheives permutation invariance of point cloud by using maxpooling as symmetric function. Transformation invariance of point cloud is acheived by generating a transformation matrx generated by Spatial Transformer Network. gloabl features are extracted by maxpooling layer and fed into segmentation head for 3D segmentation.	Point	3M
PointNet++[39]	PointNet doesnt capture local structures becuase of only global features extraction. So PointNet++ applies PointNet recursively on portions of input point cloud to extract featuers and these are grouped to form high level features.	Point	6M
TangentConv[52]	Proposes tangent convolutions which are simialr to normal convolution but an additional multiplication of gaussian kernel. The architecture is encoder-decoder style with fully convolutional network consisting of tangent convolutions.	Point	0.4M
SPLATNet[48]	This model uses Bilateral Convolutional Layers(BCL) to project data onto low dimensional lattice. These lattices from BCL are then convolved and reprojected back to the point cloud. USe of BCL allows the projection 2D semantic labels to label the 3D point cloud.	Point	0.8M
SqueezeSeg[61]	Projects the data onto 2D spherical coordinates and segmented using SqueezeNet. The segmented 2D image is reprojected back to 3d using Recurrent Conditional Random Fields.	Project	1M
SqueezesegV2[62]	Extension over SqueezeSeg by using Context Aggregation Module (CAM) before encoder to minimize the effects of missing points on convolutional filters of SqueezeSeg. Proposed novel focal loss instead of weighted cross entropy to better represent the dataset class imbalance.	Project	1M

SqueezesegV3[65]	Spherical proejction based model which uses Spatially Adaptive Convolutions to change filters according to the differnt locations in the input image. The architecture is similar to RangeNet with cross entropy loss calculated at each layer.	Project	0.92M
LatticeNet[42][1]	The input point cloud is projected onto d-dimensional sparse lattice and reprojection is learnt form the data by using novel proposed DeformSlice module. The architecture is similar to U-Net with lattice projeciton at encoder and DeformSlice at end of decoder module.	Point	-
RangeNet-21[32]	Spherical projection based model with encoder-decoder style architecture with encoder being DarkNet21. Introduced a better evaluation metric called borderIoU for occlusions.	Project	25M
RangeNet-53[32]	Architecturally similar to RangeNet-21, the only change is encoder which is DarkNet53. No postprocessing is applied for occlusions or nonprojected points.	Project	50M
RangeNet-53++[32]	RangeNet-53++ architecture is same as RangeNet-53 but a post processing method of kNN is applied on output to label the occluded points or nonprojected points after reprojection from segmented 2D spherical image to 3D points.	Project	50M
RandLA-Net[23]	Random points from input point cloud are sampled and fed into local feature aggregation (LFA) module for feature extraction. These fetures are weighted and selected based on the attention score. Encoder-decoder style architecture with stacks of LFA as encoder and decoder is transponse convolutions for upsampling with MLP followed by fully connected layers for segmentation.	Point	0.95M
3DMiniNet[2]	This model works on spherical projection of 3D point cloud which is fed into projection learning module to learn local and global features. These learnt features are fed into MiniNetV2 which is a fully connected neural network for segmentation of spherical image. This 2D image is reprojected back into 3D point cloud using kNN search as in RangeNet53++.	Project	4M
SalsaNet[1]	Encoder-decoder style architecture with Bird-Eye-View projection as input and encoder consisting of ResNet blocks and decoder with transpose convolutions. Unlabelled points in LiDAR are auto labelled from corresponding images. Claims SalsaNet is projection agnostic.	Project	6.6M

[1]LatticeNet has no code to calculate number of parameters

SalsaNext[10]	Similar architecture to SalsaNet, proposed a new context module replacing ResNet module in encoder and pixel shuffle instead of transposed convolutions in decoder. Proposed Lovasz-Softmax loss in combination with weighted cross-entropy loss. This is the first model best of our knowledge to study epistemic and aleatoric uncertainty by modelling SalsaNext as Bayesian Neural Network.	Project	6.7M
PolarNet[67]	It is a projection based model, instead of spherical or bird's eye view projection in cartesian coordinate system, this model projects the data into bird's eye view projection on to a grid of polar coordinate system. This grid is a fixed size representation and features are extracted are for each grid cell.	Project	14M
KPRNet[24]	Projects the data into 2D spherical image and 2D CNN encoder-decoder architecture is applied. Encoder consists of ResNeXt-101 and decoder is similar to DeepLab with depthwise seperable convolutions. Backprojection to 3D is made using KPConv similar to KNN in RangeNet-53++.	Project	243M
SPVNAS[50]	Proposes Sparse Point-Voxel Convolutions (SPVConv) aimed to improve performance over small objects such as pedestrains, cyclistis. SPVConv voxelizes point cloud and apply sparse convolution and then devoxelizes the voxel to point cloud. This is the first 3D semantic segmentation model to utlize Neural Architecture Search (NAS).	Point	2.6M
Cylinder3D[69][2]	Converts 3D cartesian coordinates to 3D cylinder coordinates then voxelizes and fed into Asymmetric Residual Block to extarct these cuboid features. These features are applied to 3D U-Net for segmentation.	Project	-

Table 2.2: Summary of various point and projection based 3D semantic segmentation models. In Type column point represent point based model and project represents projection based model.

We chose RandLA-Net as the model because of its ability to extract complex structures and lower parameters. Detailed reasons and explanation about RandLA-Net is discussed in Section cite here.

2.3 Uncertainty estimation methods

In this section we will discuss about existing methods to estimate uncertainty in deep neural networks. Here we divide the existing methods into ensemble methods, bayesian method and others. The methods discussed here mostly estimate epistemic uncertainty only test time augmentation and gaussian density

[2]Cylinder3D uses Sparse Convolutions which are not supported in Ubuntu-20 at the time of study.

models estimate aleatoric unceratinty.

2.3.1 Ensemble methods

Deep ensembles first proposed in [27] are the most prominently used methods for the uncertainty estimation. They exploit the combinatory power of multiple models. Each input is fed into a model with multiple instances and the each instance of the model is initalized randomly. This leads to slightly different optimization for each of the instance of the model. The final output scores from each model are combined by simple averaging. Deep ensembles are known to improve overall performance of the model but comes with a cost of computational complexity and resource intensiveness. Another advantage of using deep ensembled are the lowest correaltion between the model instances as the training of the instances are done differently. This lower correlation figures lead to diverse prediction from each model instance. In detailed explantion about deep ensembles can be found in Chapter cite Section cite.

Because of the higher computational complexity and resource intensiveness, multiple flavours of the deep ensembles are proposed such as deep sub-ensembles cite and masksembles cite. In deep sub-ensembles, the network is divided into two parts called trunk and head. The main idea here is to train multiple instances of the head with the same trunk. For example, a trunk can be feature extraction layers in a deep classification network and the head can be the classification layers. Since the major motivation of the subensembles is to improve the training speed the performance lacks minutely when compared to deep ensembles as it is a tradeoff between the computational time and quality of uncertainty. Masksembles proposed in cite are realtively new and are a combination of deep ensembles with MC-Dropout. Dropout proposed in cite includes dropping of random neurons where as here a predefined mask is stated for each layer and only those certain neurons are to be dropped everytime.

Other methods include snapshot ensembles cite which iterates over the multiple local optima in the optimization landscape using cyclic learning rate. The model parameters are saved at each of the local optima. All of the other flavors of deep ensembles are proposed in order to reduce the effect on time but the memory requirements remain mostly the same except the subensembles. The other problem with snapshot ensembles are the optimization landscape in deep neural networks are poorly studied, so there one cannot say with certainty that model saved at two local minima are uncorrelated. There also exists neural ensemble search cite where the nerual archiecture search is applied over the ensembles. Instead of using various instances of the same model, authors in cite above paper use vaiours instances of various models in the archiecture search space. Finally, all the above discussed ensmeble models can be group under sampling based methods, because each image is passed to mulitple model instances.

2.3.2 Bayesian methods

Existing neural networks are trained in maximum likelihood manner resulting in a point estimates for the weights. The main idea behind bayesian neural networks are to use a distribution over the network parameters. That is instead of single fixed weight tesnor for a layer in neural network, a weight tensor

is drawn from the distribution for each forward pass. The parameters are estimated for input during training by using bayes rule and expressed in Equation cite eq here.

$$p(\theta|x,y) = \frac{p(y|x,\theta)p(\theta)}{p(y|x)} = \frac{p(y|x,\theta)p(\theta)}{\int p(y|x,\theta)p(\theta)d\theta}$$

Here θ represents network parameters (weights), $p(\theta)$ represents prior distribution over θ, and x and y represents the input data, in our case point cloud and its corresponding semantic point labels During inference, the labels are calculated by bayesian model averaging as given in below equation.

$$p(y_t|x_t,x,y) = \int p(y_t|x_t,\theta)p(\theta|x,y)d\theta$$

Here θ represents trained network parameters, x and y represents training set, and x_t and y_t represents the test set. The integral in the Equation cite eq here cannont be computed because θ is the continous space and so iterating over all possible values of θ are not feasible. So to acheive tractable θ, there exists various approximation methods such as Variational Inference (VI), Laplace approxoimation and sampling methods such as Monte Carlo sampling.

VI is a approximation method where the posterior probability $p(\theta|x,y)$ is approximated by specific distribtions represented by $q(\theta)$. Kullback-Liebler Divergence (KLD) is used as a measure to calculate the difference between the two distributions. Since KLD cannot be optimized directly becuase of posterior distribution, a function called Evidence Lower BOund (ELBO) similar to KLD is proposed. cite represented the $q(\theta)$ as a gaussian approximation and cite proposed bayes by backprop to extend stochastic VI for non gaussian priors. cite provides stochastic variational inference that is ELBO loss over mini-batch of data and also assumed the network parameter priors are to be gaussian. cite makes use of reparameterization trick for reduction in variance in gradients. This lead to reformulation of ELBO loss which made it compatible to standard backpropogation. Talk about normalizing flows.

Another widely known example for VI is Monte Carlo Dropout (MC-Dropout), in which the dropout layers are reformanulated as random variables with Bernoulli distribtion. and as in cite here and swaroop work that training with dropout layers can be formulated as VI and predictive uncertainty can be calculated during inference by applying MC-Dropout during inference. The other flavour of MC-Dropout is the random incoming activations to the node are dropped instead of nodes themselves and this methods is called Monte Carlo Dropconnect (MC-Dropconnect) as proposed in cite. An example of MC-Dropout and MC-Dropconnect is depecited in Figure cite.

Another method for estimating uncertinty is flipout as proposed in cite. Although flipout was proposed to decorrelate gradients in a minibatch by sampling independent weight perturbations for each example, it is used for variational inference as in cite. Sampling methods also called as Monte Carlo methods (not to be confused to Monte Carlo Dropout or Monte Carlo Dropconnect) estimate uncertainty without any approximation of parametric model. The most popular method in the category of sampling methods is Markov Chain Monte Carlo (MCMC) sampling proposed in cite. Hamiltonian Monte Carlo (HMC) is an another variant of MCMC method and is considered as gold standard algorithm for Bayesian inference

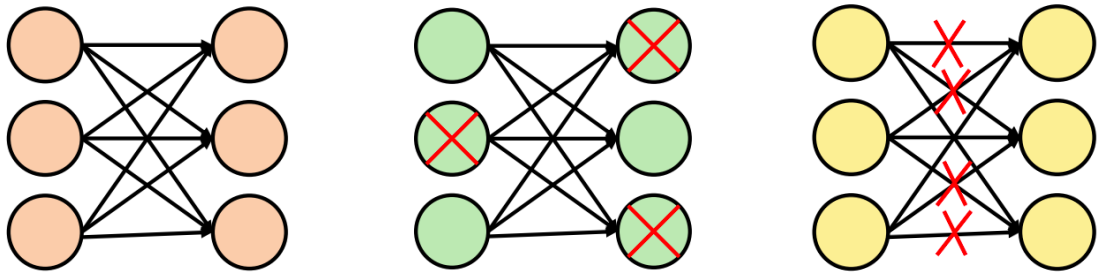

(a) (b) (c)

Figure 2.4: Images taken from cite

as stated in cite. Laplace approximaiton methods make use of second order Tayler series approximation to estimate $p(\theta|x, y)$. Uncertianty in the laplace approximation methods is calculated by taking Hessian matrix of $log(p(\theta|x, y))$ and can be applied to existing trained neural networks as in cite. Sampling methods and laplace approimation methods arenot studied because the former is computationally expensive and later suffers from infeasibility to compute Hessian matrix for deep neural networks.

2.4 Out-of-distribution (OOD) detection methods

In this section, we will discuss about the existing OOD detection methods for 2D classification task and 2D semantic segmentation task. To the best of our knowledge, ours is the first work to study OOD detection for the task of 3D semantic segmentation.

The most widely used benchmarked datasets used for 2D classficiation dataset are CIFAR-10 vs SVHN cite, CIFAR-10 vs LSUN cite, abd MNIST vs Fashion-MNIST cite. Most of the proposed methods for OOD detection in classification tasks are threshold based methods. These methods employ a threshold based detector and does not see the OOD data during the training. The baseline method for threshold based methods is proposed in cite. cite uses Maximum Softmax Probability (MSP) and argues that in distribtion dataset have higher softmax score and out of distribtion dataset have lower softmax score and computed as in Equation 2.1 where $f_i(x)$ is the output of neural network. Since the softmax scores can be overconfident cite proposed Out of DIstribution detector for Neural networks (ODIN) which makes use of calibrated softmax score by addition of temperature constant to softmax scores and computed as in Equation 2.2 where $f_i(x)$ is the output of neural network and T is the temperature constant for calibrated softmax scores. In addition to calibrated softmax scores, ODIN also adds noise perturbations to the input making the training adversarial. ODIN needs access to the OOD samples because the finetuning of perturbation magnitude is made based on these samples.

$$S_{MSP}(x) = max_i \frac{exp(f_i(x))}{\sum_{j=1}^{C} exp(f_j(x))} \tag{2.1}$$

$$S_{ODIN}(x) = max_i \frac{exp(f_i(x)/T)}{\sum_{j=1}^{C} exp(f_j(x)/T)} \tag{2.2}$$

cite has proposed a threshold based OOD detection method using the Mahalanobis distance as confidence score. The mahalanonis distance is calculated for every layer of the network and these individual Mahalanobis scores are combined to get confidence score. TODO:

1. Form the Story
2. Write it out

3

Datasets and Benchmarking

3.1 Semantic3D

Semantic3D is a huge 3D benchmark point cloud classification dataset and classified as static dataset. The dataset consists of nearly 4 billion points which contain variety of scenes in urban and rural setting. These scenes are taken in places such as markets, dom, stations and fields collected in European streets with terrestrial lasers. Each point in the point cloud consists of geometric positions (x, y, and z), color (R, G, and B) and intensity values as features. Example point cloud scenes are provided in Figure **??**.

The dataset consits of 8 classes and they include

1. man-made terrain - pavement
2. natural terrain - grass
3. high vegetation - large bushes and trees
4. low vegetation - flowers and bushes less than 2cm in height
5. buildings - stations, churches, cityhalls
6. hardscapes - garden walls, banks, fountains
7. scanning artificats - dynmically moving objects
8. cars

The distribution of these calsses are given in Figure 3.1. From this graph, we can observe that the manmade terrain made most of the dataset because the lidar is placed on street during collection. As they are near to lidar and it is common with outdoor lidar datasets. The classes low vegetation, hardscapes, scanning artificats and cars have less number of training points and lower performance from the model on these classes are to be expected. Also according to [19], scanning artifacts, cars and hardscapes are toughest classes becuase of variation in obejct shapes. [13] also proves that the Semantic3D is most diverse dataset in 3D LiDAR data compared to other datasets such as SemanticKITTI and SemanticPOSS. Becuase of these reasons, we considered using Semantic3D dataset as in distribution training data. The dataset is available to download on http://www.semantic3d.net/. As this is an ongoing benchmark challenge, the

labels for the testing data is not available. We made use of validation set for evaluation purpose which is a subset of trianing set.

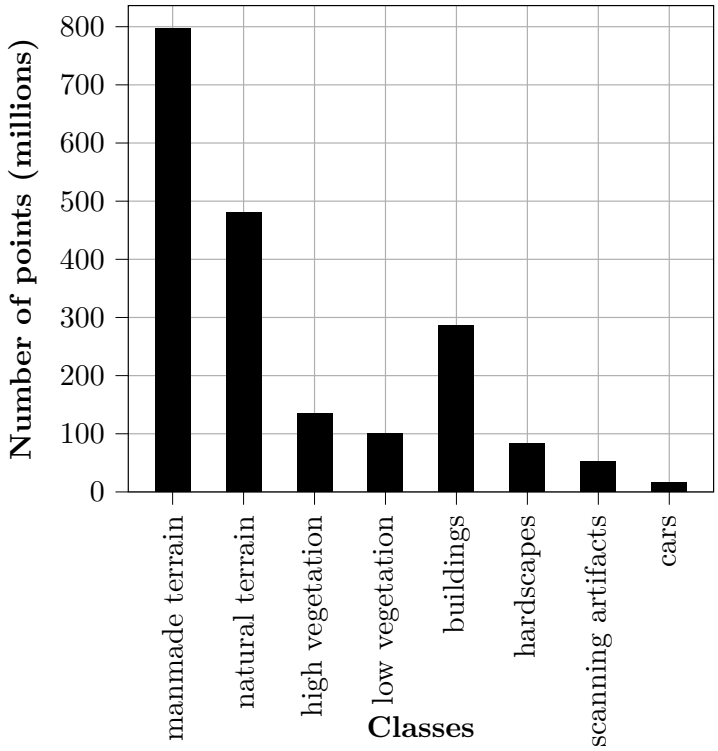

Figure 3.1: Distribution of training points in million per class in Semantic3D dataset.

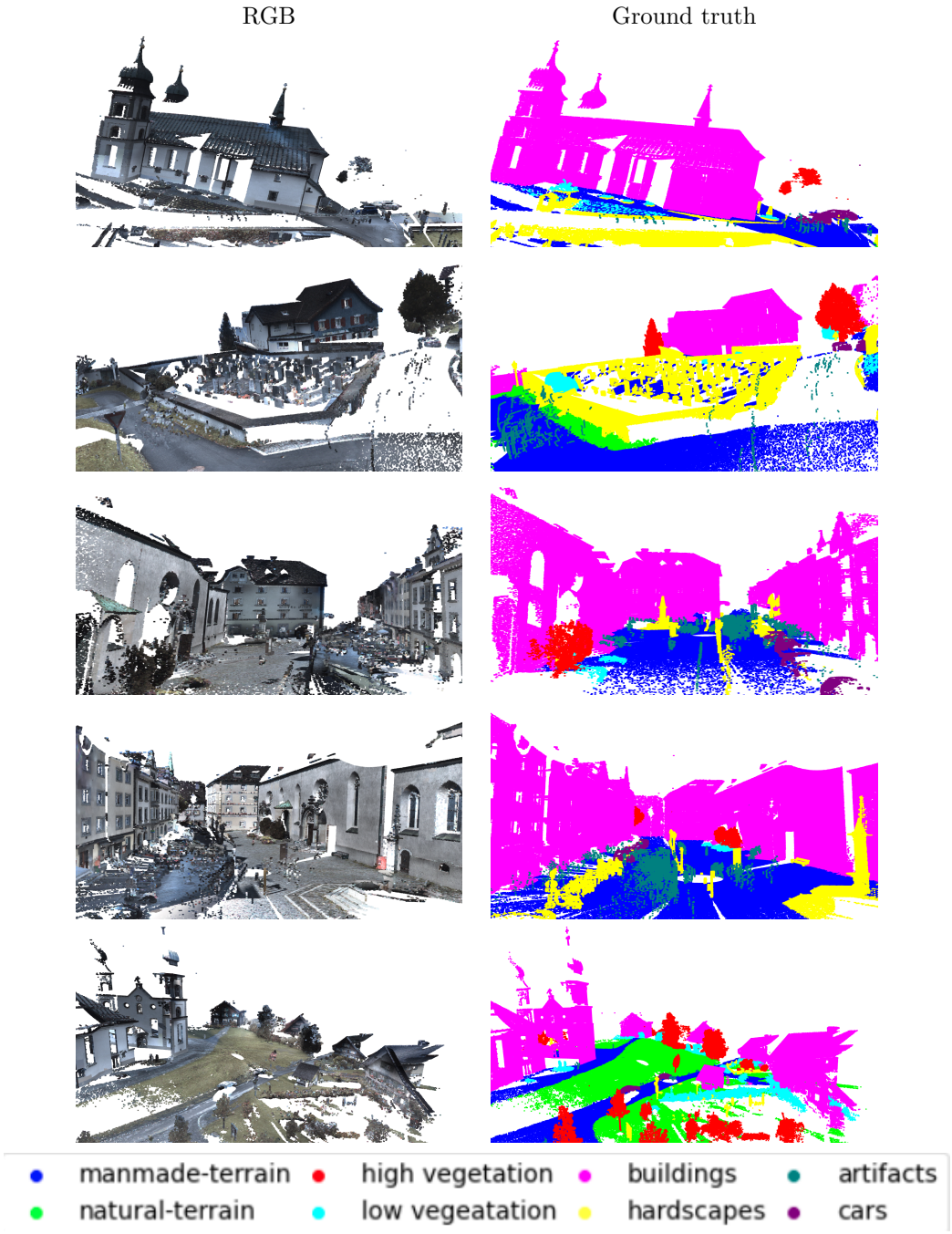

Figure 3.2: Illustration of point clouds in training and validation set with first column representing RGB colors of point cloud and second columns their ground truth colors with legend given in last image.

3.2 S3DIS

S3DIS is an indoor dataset making it an ideal OOD dataset candidatae becuase of the no class overlap with the Semantic3D dataset. It is only one of two datasets available in indoor LiDAR dataset candidataes. The other is ScanObjectNN whose dataset is not available online. S3DIS dataset comprises of scans of three different buildings covering an 6020 square meters. These scans include areas such as personal offices, restrooms, open spaces, lobbies and hallways. The scans are generated using Matterport 3D scanner and can be seen in **cite figure**. S3DIS dataset is divided into 12 classes which are further divided into two subclasses. First subclass include structural elements which consist of *ceiling, floor, window, wall, beam, columns and door* and latter subclass has common items such as *table, sofa, chair, board and blackboard*. Along with ShapeNet dataset, S3DIS is also one of the most evaluated dataset in indoor setting for semantic segmentation using in cite S3DIS papers here whereas ShapeNet is used for part segmentation.

4

Methodology

In this chapter, we will discuss about RandLA-Net used for 3D semantic segmentation, especially about how the RandLA-Net architecture helps in efficient segmentation. How random point sampling along with local feature aggregation module in RandLA-Net is better than other sampling methods. We also discuss about the deep ensembles for uncertinty quantification and, we conclude this chapter with the environment and training details for the RandLA-Net with deep ensembles.

4.1 RandLA-Net

As stated in [23], it is a light weight, and efficient neural network architecture for sematic segmentation of 3D point clouds. From related work section **refer section here**, we can observe that the RandLA-Net architecture is best performing among the point models. Efficient computation, memory usage and a model with direct application o 3D points are the main motivation when developing the RandLA-Net. To acheive these goals, RandLA-Net employs random point sampling along with the local feature aggregation module. Authors in [23] proved that by a successive application of random point sampling along with lcoal feature aggregation module effective reduce and extract the features of the large scale point clouds from a scale of 10^5 to 10^2.

RandLA-Net utilizes random point sampling among the other sampling methods such as Farthest Point Sampling, Inverse Density Point Sampling. In random point sampling, we select K points uniformly from original point cloud and has a computational complexity time of O(1). When compared among other point sampling methods, random point sampling has the lowest computational complexity and computation time is completely independent on number of points. Despite of these advantages, random point sampling comes with a major disadvantgae of important points being dropped. To overcome this, authors of RandLA-Net proposed local feature aggragation module for progressive capture of complex features on these selected points.

Figure 4.1a represents the local features aggregation module for the RandLA-Net. This module is applied paralelly on the 3D points and architecture of local feature aggregation module is further divided into three sub modules. They are local spatial encoding (LocSE), attentive pooling and dilated residual block represented as green, pink and blue blocks respectively in Figure 4.1a. Let us discuss further each of these submodules in detail.

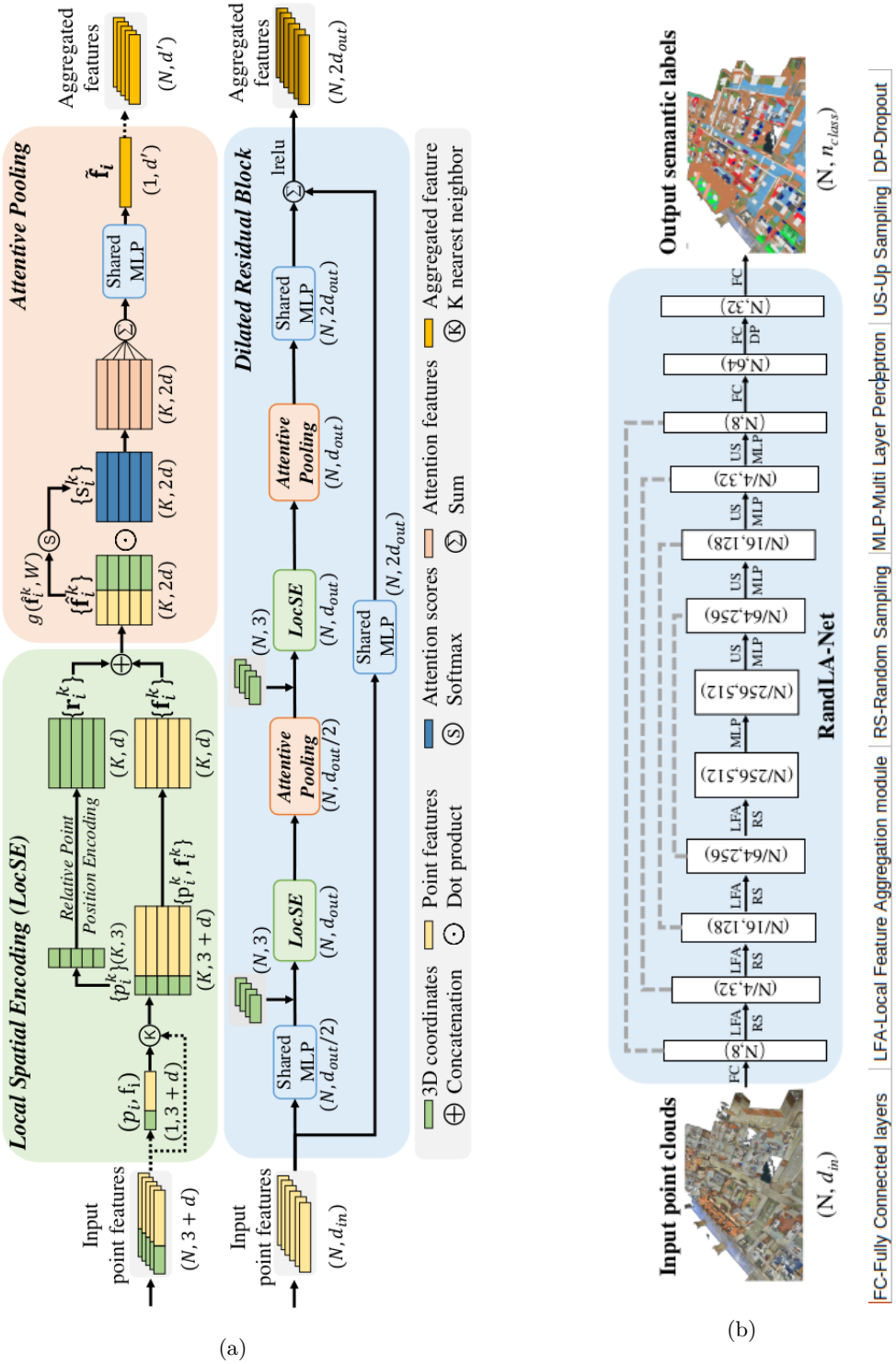

(a) (b)

Figure 4.1: Illustration of (a) local feature aggregation module in RandLa-Net and (b) architecture of RandLA-Net. Both the images are taken from [23]

4.1.1 Local Spatial Encoding (LocSE)

Local spatial enconding module takes each point (p_i) in point cloud (P) and encodes its neighbouring points position(x, y and z). This encoding makes sure that point p always have information of its neighbours. Also this encoding helps in learning geometric patterns and learn complex structures progressively. This module works in three steps:

1. Finding nearest neighbours

2. Relative position encoding

3. Feature augmentation

In step 1, neighbouring points for point (p_i) are collected using euclidean distance based K-nearest neighbour (KNN) algorithm. Step 2 encodes these collected K-points for point (p_i) using a Multi Layer Perceptron (MLP) into realtive point position. The encoding formula is given by

$$r_i^k = MLP(p_i \oplus p_i^k \oplus (p_i - p_i^k) \oplus ||p_i - p_i^k||)$$

where r_i^k is the relative position of point p_i with respect to p_i^k, here in p_i and p_i^k only the x,y and z positions are used. $\oplus$, and $||p_i - p_i^k||$ represents the concatenation operation and euclidean distance calculation between p_i and p_i^k respectively. This step 2 of relative position encoding is represented by above part in LocSE module in green track in Figure 4.1a. Step 3 creates a augmented feature vector $\hat{f_i^k}$ by concatenation of relative point position (r_i^k) and its point features (f_i^k) of point p_i^k. Point features (f_i^k) include the R,G and B values and other features such as intensity values. This step 3 is represented in lower part of the LocSE module in yellow track in Figure 4.1a.

4.1.2 Attentive Pooling

This augmented feature vector $\hat{f_i^k}$ from LocSE module is passed through a pooling layer to extract important features. Authors state that use of max and mean pooling layer leads in loss of information, because of this authors made use of attention mechanism which helps in learning important features automatically. Given the feature vector $\hat{f_i^k}$ a function g is learned by help of MLP and softmax and the resultant vector is denoted as s_i^k in the pink block in Figure 4.1a. These each feature score s_i^k from function g is multiplied with feature vector f_i^k called informative feature vector and summed up to form a unique feature vector $\tilde{f}_i$ for point p_i and this operation is mathematically denoted as

$$\tilde{f}_i = \sum_{k=1}^{K} (\hat{f_i^k} . s_i^k)$$

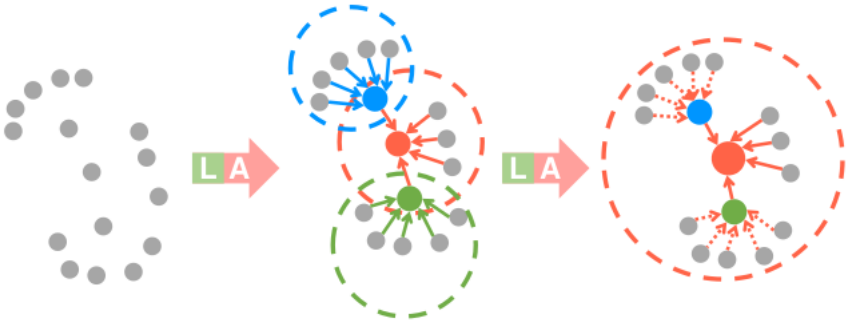

Figure 4.2: Dilated residual block. Image taken from [23].

4.1.3 Dilated Residual Block

Dilated Resudial Block is a ResNet inspired module as claimed by authors and represented as blue color module in Figure 4.1a. This module is a combination of multiple LocSE, Attentive Polling, and a skip connection which feeds informative feature vector to output. Let us consider a red point in Figure 4.2 and after application of first LocSE and Attentive Pooling module it observes K neighbours represented in red circle. Secondary application of LocSE and Attentive Polling allows the red point to observe K^2 neighbours represented as large red circle in right subimage in Figure 4.2. This progressive dilation of receptive fields allows to observe local features in first application of LocSe and Attentive Pooling and then observe global features on further application of LocSE and Attentive Polling modules. Authors claim that more LocSE and Attentive Pooling stacked in Dilated Residual Block powerful the Dilated Residual Block becomes and greater the receptive field at an expense of computational time. Authors also claim that only by stacked application of two LocSE and Attentive Pooling modules is powerful enough and it is effective and efficient in computational time.

To summarize upto this point, we have studied the special feature of RandLA-Net. That is how random point sampling in conjecture with local features aggregation module in Figure 4.1a helps in extraction of features progressively. We also studied how local feature aggragation module is divided into three sub modules namely Local Spatial Encoding (LocSE), Attentive Pooling and Dilated Residual Block and each of this submodules working procedure. In the next section we study the architecture of RandLA-Net.

4.1.4 RandLA-Net architecture

RandLA-Net is an encoder-decoder architecture with skip connections as used in various segmentation networks such as 3D U-Net[59]. The input point clouds are directly applied to encoder consisting of Fully Connected (FC) and four Local Feature Aggragation (LFA) modules connected sequentially. The size of point cloud reduces by a factor of four for every encoder layer. Similarly four decoder layers are used and the input features maps to each decoder layer is upsampled and concatenated to respective encoder feature maps via skip connections. The MLP is applied and fed into next decoder layer. Output of final

decoder layer is fed in to three FC layers for point classification and a dropout layer is added before last layer with a dropout rate of 0.5. The detailed network architecture is illustrated in Figure 4.1b.

We chose RandLA-Net because of the following reasons:

1. Efficient extraction of complex structures progressively using Local Feature Aggregation (LFA) module.

2. Has lower number of parameters (1.24M) making training efficient, as 3D semantic segmentation models are computationally expensive.

3. Proven performance over variety of datasets such as Semantic3D and SemanticKITTI, along with ablation study of each submodule in LFA proposed in [23].

4. No preprocessing such as range image representation as in [32] or farthest point sampling with a computaitonal complexity of $O(N^2)$ as in [38]. Whereas RandLA-Net employs random point sampling with computational time of $O(1)$.

5. State of the art performance in point based methods, consisting of only Multi Layer Perceptrons (MLP) and without expensive operations such as kernalization or graph construction.

4.1.5 Evaluation metrics

To evaluate the performance of RandLA-Net over the training dataset (Semantic3D in our case) we chose two metrics. They are Mean Intersection-over-Union (mIoU) and Accuracy.

Mean Intersection-over-Union (mIoU)

Mean Intersection-over-Union is a widely used metric for performance evaluation in task of semantic segmentation. It is calculated as mean of fraction of intersection area between predicted and ground truth masks and union of predicted and ground truth masks. mIoU is calculated as

$$mIoU = \frac{1}{N} \sum_{k=1}^{N} \frac{p_k \cap g_k}{p_k \cup g_k}$$

where N is the number of classes, p_k and g_k are predicted mask and ground truth mask of k^{th} class.

Accuracy

Accuracy is another wide used metric, which can be quantified as number of points in the point cloud correctly classified. It can be formulated from confusion matrix as

$$Accuracy = \frac{TP + TN}{TP + TN + FP + FN}$$

where TP, TN, FP and FN are True Positives, True Negatives, False Positives and False Negatives respectively from the confusion matrix. This metric alone can be misleading in case of serious class imbalance.

Here, we conclude the study of RandLA-Net, reason for its effective performance, argued the reasons to chose RandLA-Net and briefly discussed evaluation metrics used. In following sections we will discuss about the utilized uncertainty estimation methods such as deep ensembles, **complete this**

4.2 Deep ensembles

Deep ensembles employ kind of ensemble learning technique and proposed in [27]. Similar to bagging, here the idea is to train the same network with same data with random initializations N number of times. These N trained models converge similarly with little difference given the same trianing conditions and hyperparameters. An example of deep ensemble is depicted in Figure 4.3. Here the input point cloud is fed into N number of models, in our case these models are all RandLA-Net. The resulting predictions are combined to get the final prediction. The combination is done by averaging over all the predictions of N models to get final predictions in our case. the detailed training algorithm is given in appendix **cite appendix here**. Deep ensembles are proven to improve the overall performance of the model as in [6] and we also expect same behaviour in our case.

Inspite of their performance boosting ability, they are also used to esitamtie uncertainty as in [27]. With the increase in number of ensembles, the Negative Log-Likelihood (NLL) and Brier score goes down suggesting network produces well calibrated predictions. [27] also study the effect of entropy with out-of-distribution (OOD) classes. They performed the study on MNIST-NotMNIST, and SVHN-CIFAR10 with first dataset in pair being in distribution (ID) and second dataset is OOD dataset. Authors verified that the distribution of entropy on ID dataset is peaky and similarly the distribution of entropy on OOD dataset is more spread across all entropy values. We hypothesize, that similar performance is observed in 3D semantic segmentation as task of segmentation can be treated as multi class classification in a point cloud. Because of proven ability to classify OOD on classification task, boost the performance of the model and ease of implementation makes deep ensembles an ideal candidate for OOD detection in 3D semantic segmentation.

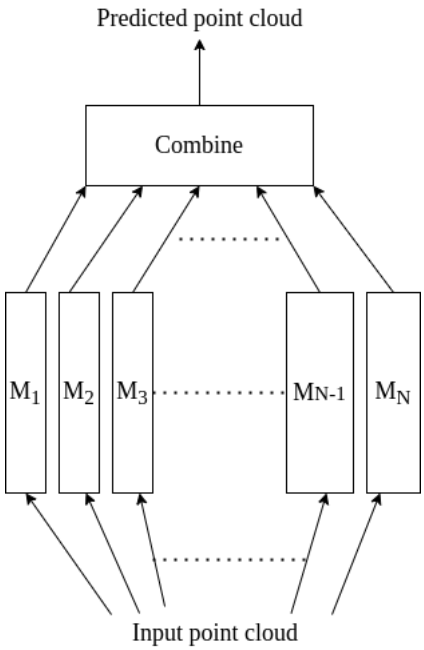

Figure 4.3: Deep ensembles

5

Solution

Your main contributions go here

5.1 Proposed algorithm

5.2 Implementation details

6

Evaluation

Implementation and measurements.

7

Results

In this chapter, we will discuss about the experiments conducted for out-of-distribution (OOD) detection on RandLA-Net using uncertainty techniques such as deep ensembles and flipout. These experiments were conducted on Semantic3D dataset as training in-distribution (ID) dataset and two datasets particularly S3DIS and Toronto3D are used as OOD datasets. The detailed description about datasets can be found in Chapter cite here, about RandLA-Net in Section cite here, and about deep ensembles and flipout in Section cite here The list of experiments conducted to acheive OOD detection are as follows:

1. Train and evaluate the deep ensembles of RandLA-Net on Semantic3D dataset and discussed in Section 7.1.

7.1 Deep ensembles

Aim: Train multiple models of RandLA-Net with random initializations on Semantic3D dataset and combine the results from the get combined prediction. These models are evlauated using mean Intersection-over-Union (mIOU) and Accuracy.

		IoU per class								
#Ensembles	**MeanIOU**	**C1**	**C2**	**C3**	**C4**	**C5**	**C6**	**C7**	**C8**	**Accuracy**
1	68.19	94.55	81.19	84.67	29.43	81.37	18.85	64.74	90.74	88.78
5	69.51	94.73	81.92	84.42	28.05	**86.41**	28.50	61.03	91.03	90.04
10	69.97	95.25	83.73	86.63	30.36	84.13	18.60	**66.01**	92.61	89.94
15	70.32	95.27	83.54	**88.22**	**32.19**	84.82	26.17	61.67	90.75	**90.57**
20	**70.80**	**95.55**	**84.11**	86.65	29.60	85.41	**29.58**	62.47	**93.06**	90.56

Table 7.1: Illustration of performance of RandLA-Net on Semantic3D over number of ensembles. meanIOU and IOU per class and overall accuracy are represented here. C1 to C8 are the classes of Semantic3D which are Manmadeterrain, Naturalterrain, Highvegetation, Lowvegetation, Buildings, Hardscapes, Scanningartifacts, and Cars.

We trained 20 models of RandLA-Net over Semantic3D dataset with training procedure described in Section cite here. Table 7.1 represents the meanIoU, Accuracy and per class IoU with each row representing the performance value with ensemble size being multiple of 5. Figure 7.1a and 7.1b representing the performance with mIoU and Accuracy with all ensmebles respectively. Some of the predicted points clouds in comparison with ground truth are represented in Figure cite here.

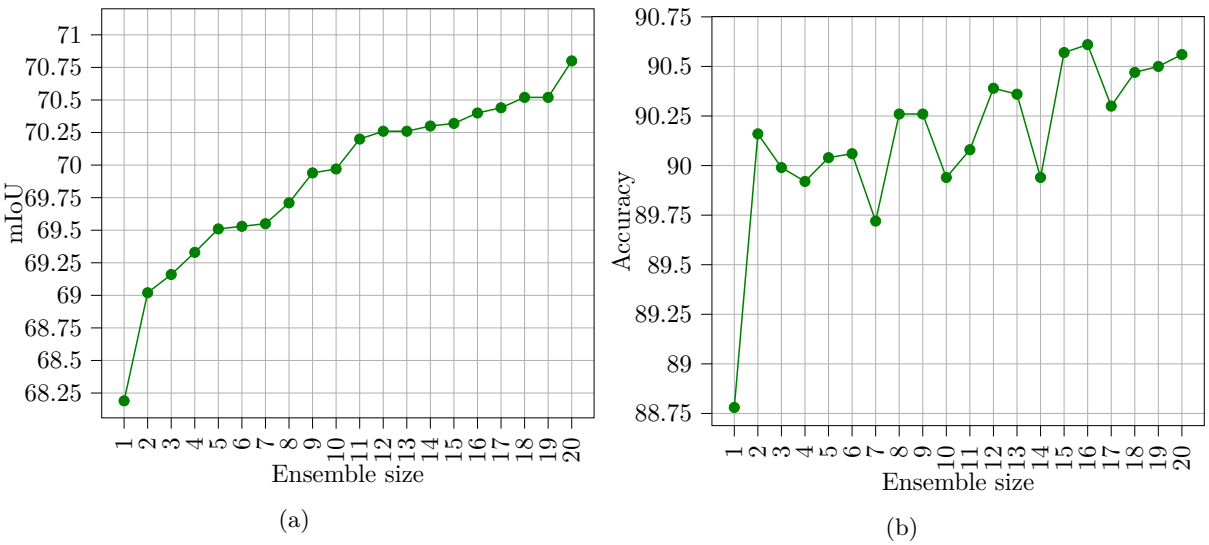

Figure 7.1: Evaluation results of the deep ensemble of RandLA-Het on Semantic3D dataset with (a) representing the meanIoU over ensemble size and (b) representing accuracy over ensemble size.

Conclusions: From this experiment, we draw the following conclusions

- Deep ensembles improved the overall performance of the model significantly in terms of mIoU and Accuracy.
- Figure 3.1 depicts low training points size for classes low vegetation, hardscapes, scanning artifacts and cars. Because of this classes low vegetation and hardscapes show less mIoU but use of deep ensembles improved their performance significantly.
- Eventhough cars are underrepresented in number of training points, efficient feature extraction of RandLA-Net helps in better segmentation of cars. As this is the same case in SemanticKITTI evaluation proposed in [23].
- From Figure 7.1a, the performance gains in terms of mIOU after the ensemble size of 10 is minimal.

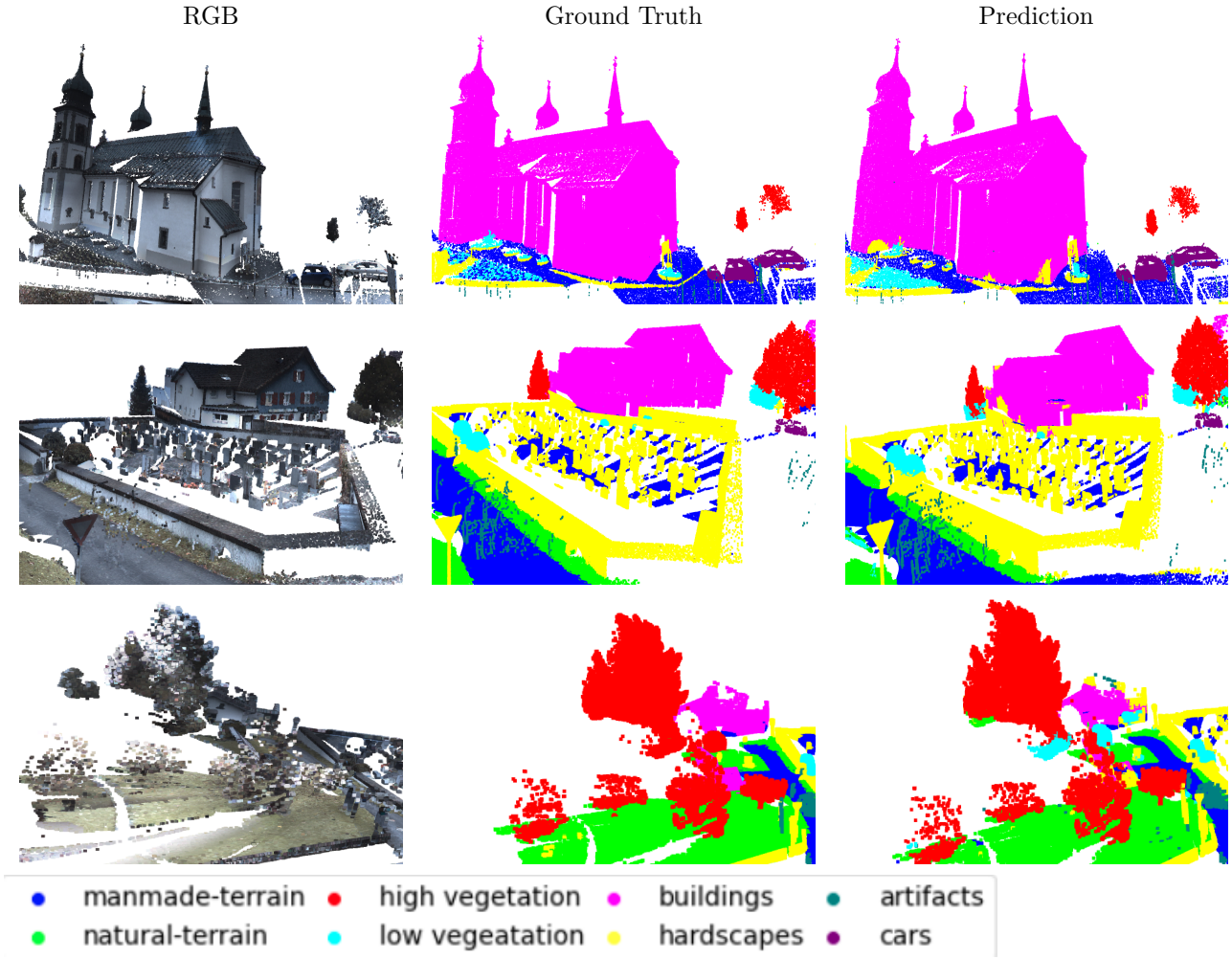

Figure 7.2: Output predictions of the RandLA-Net over the Semantic3D dataset.

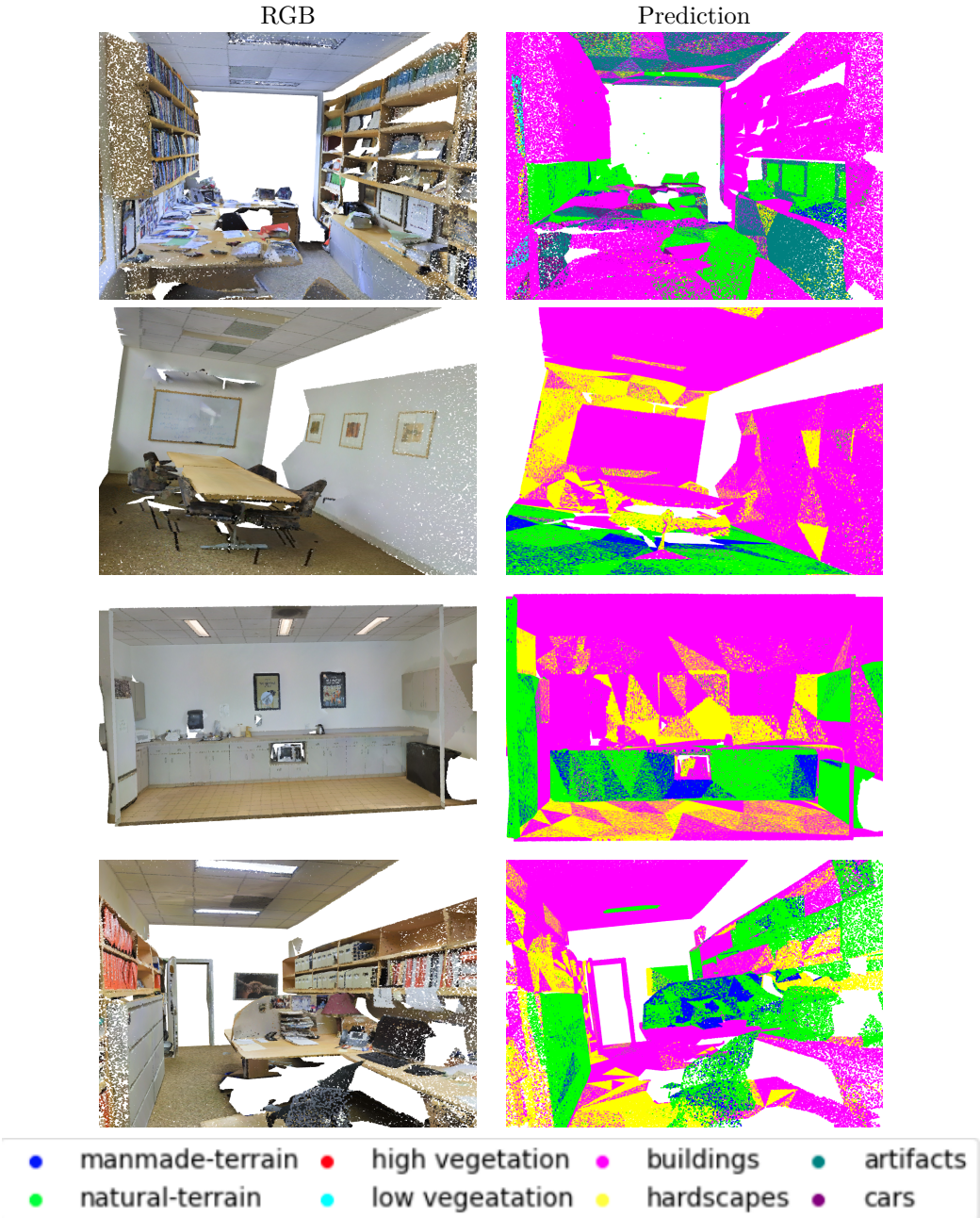

Figure 7.3: Output predictions of the RandLA-Net over the S3DIS dataset.

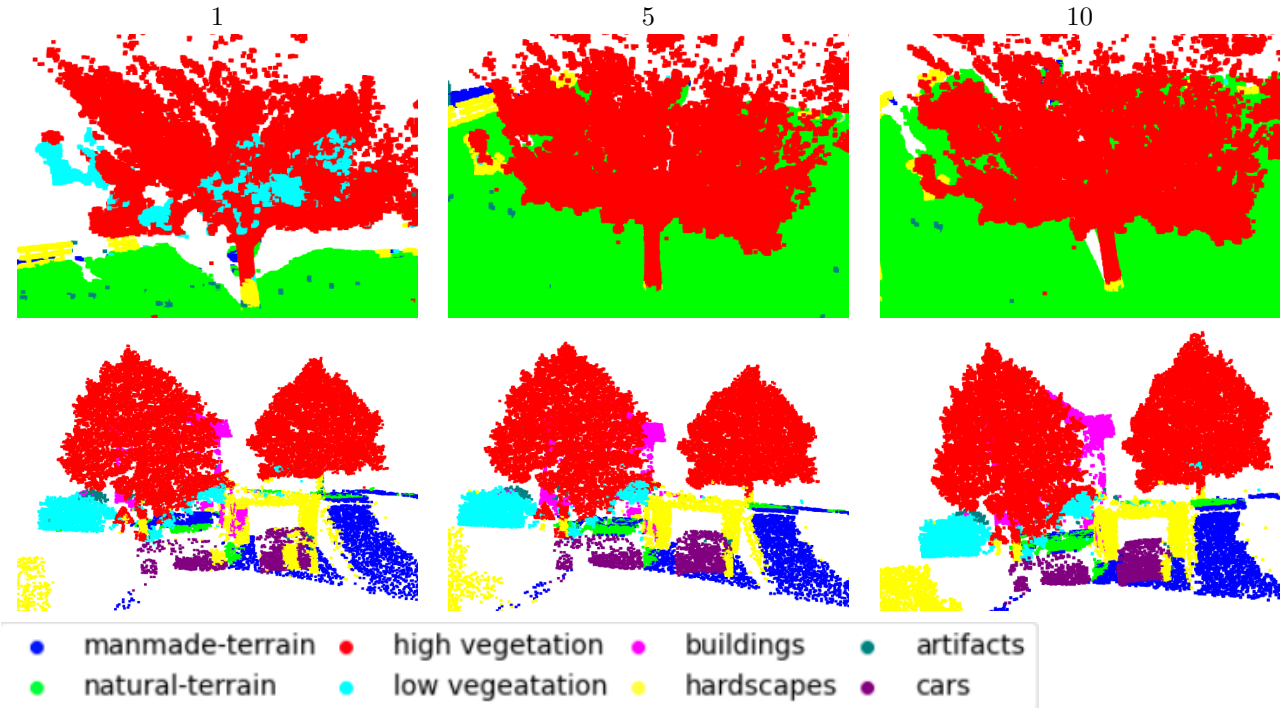

Figure 7.4: Deep ensembles performance on RandLA-Net over the Semantic3D dataset.

7.2 Probability-Semantic3D vs S3DIS

Aim: In this experiment, we study how the probability scores are distributed in Semantic3D and S3DIS datasets which are ID and OOD datasets respectively.

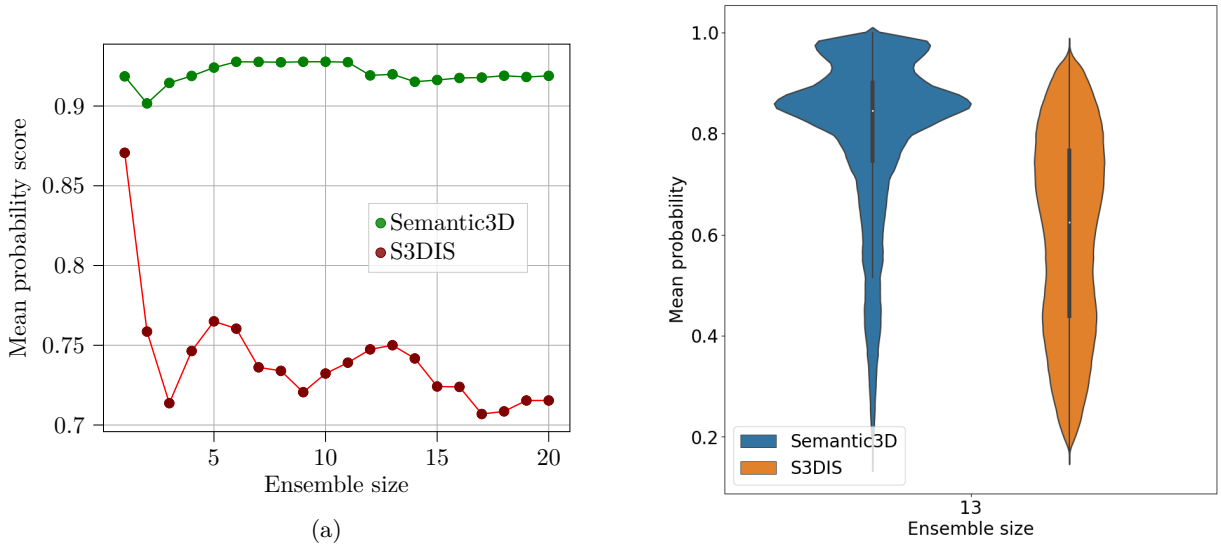

(a) (b)

Figure 7.5: Plots depicting how probability score with ensemble size 7.5a representing average probability score and how does it change with ensemble size, 7.5b depicting the distribution of the probability scores.

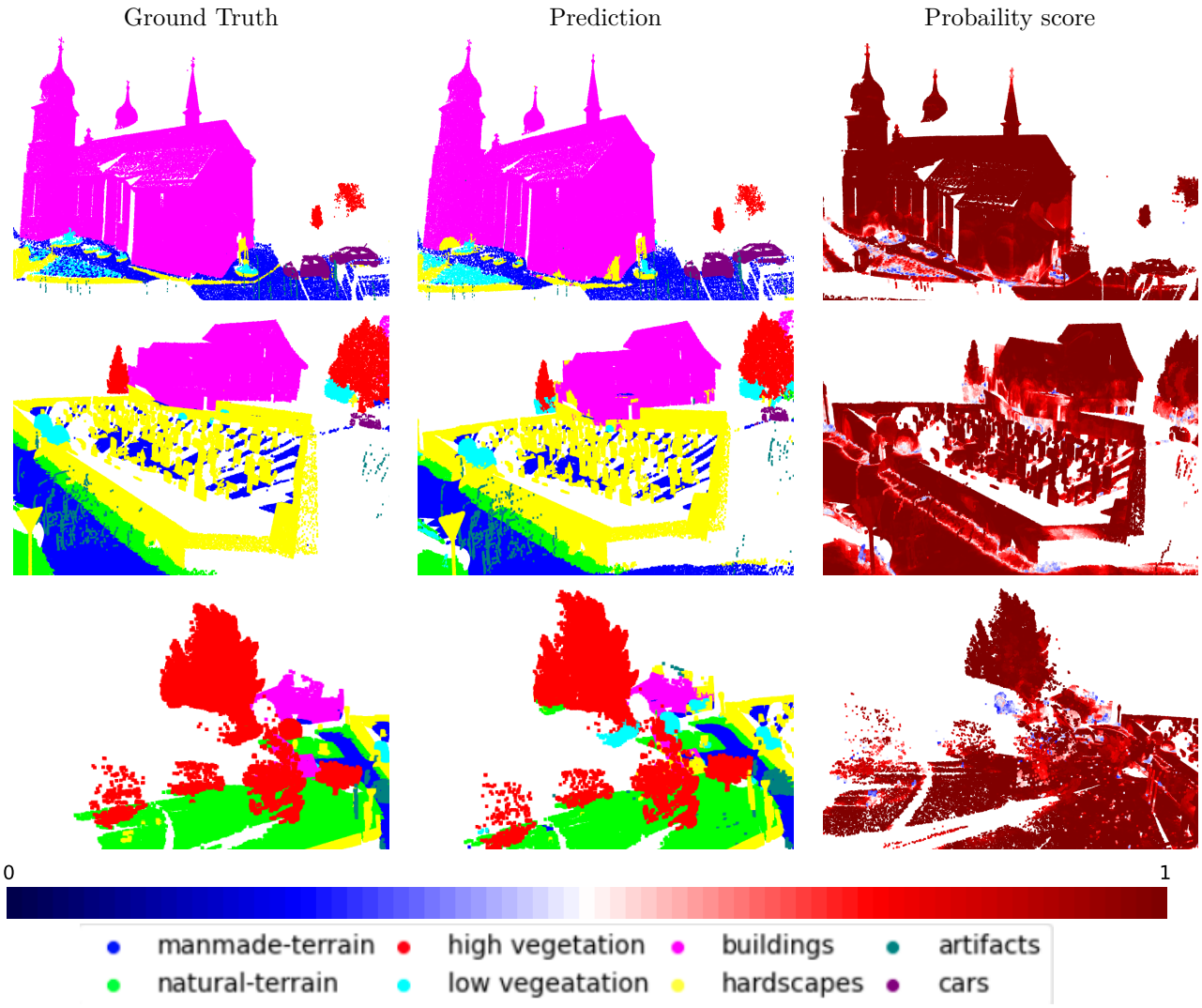

Figure 7.6: Perpoint probability visualization of the semantic3D dataset.

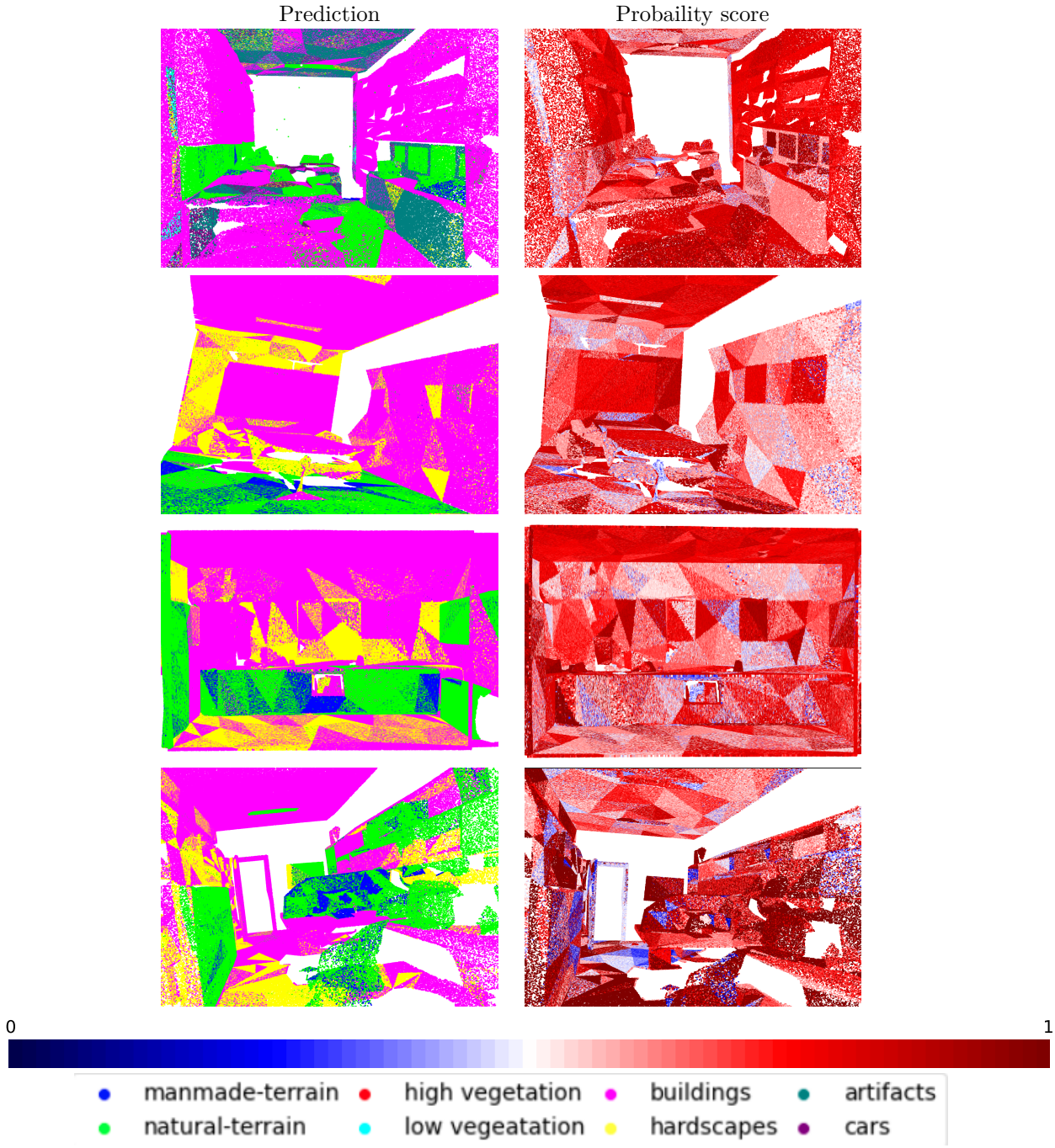

Figure 7.7: Perpoint probability visualization of the S3DIS dataset.

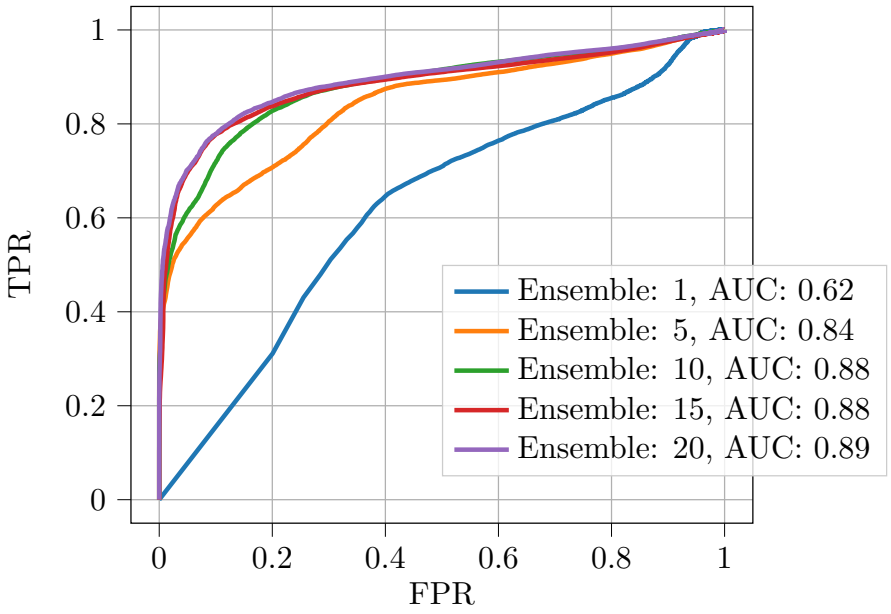

Figure 7.8: ROC plots and AUROC scores for maximum probability in semantic3D vs S3DIS

7.3 Entropy-Semantic3D vs S3DIS

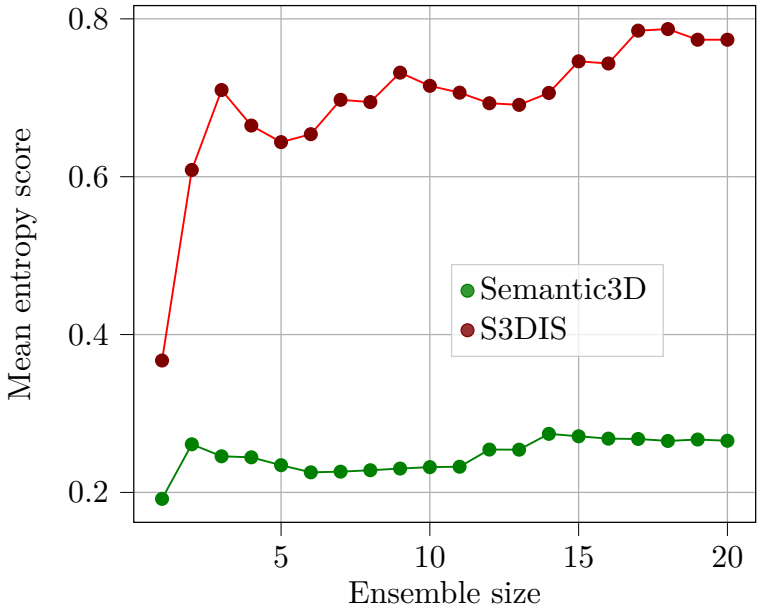

Figure 7.9: Plots depicting how entropy changes with ensemble size

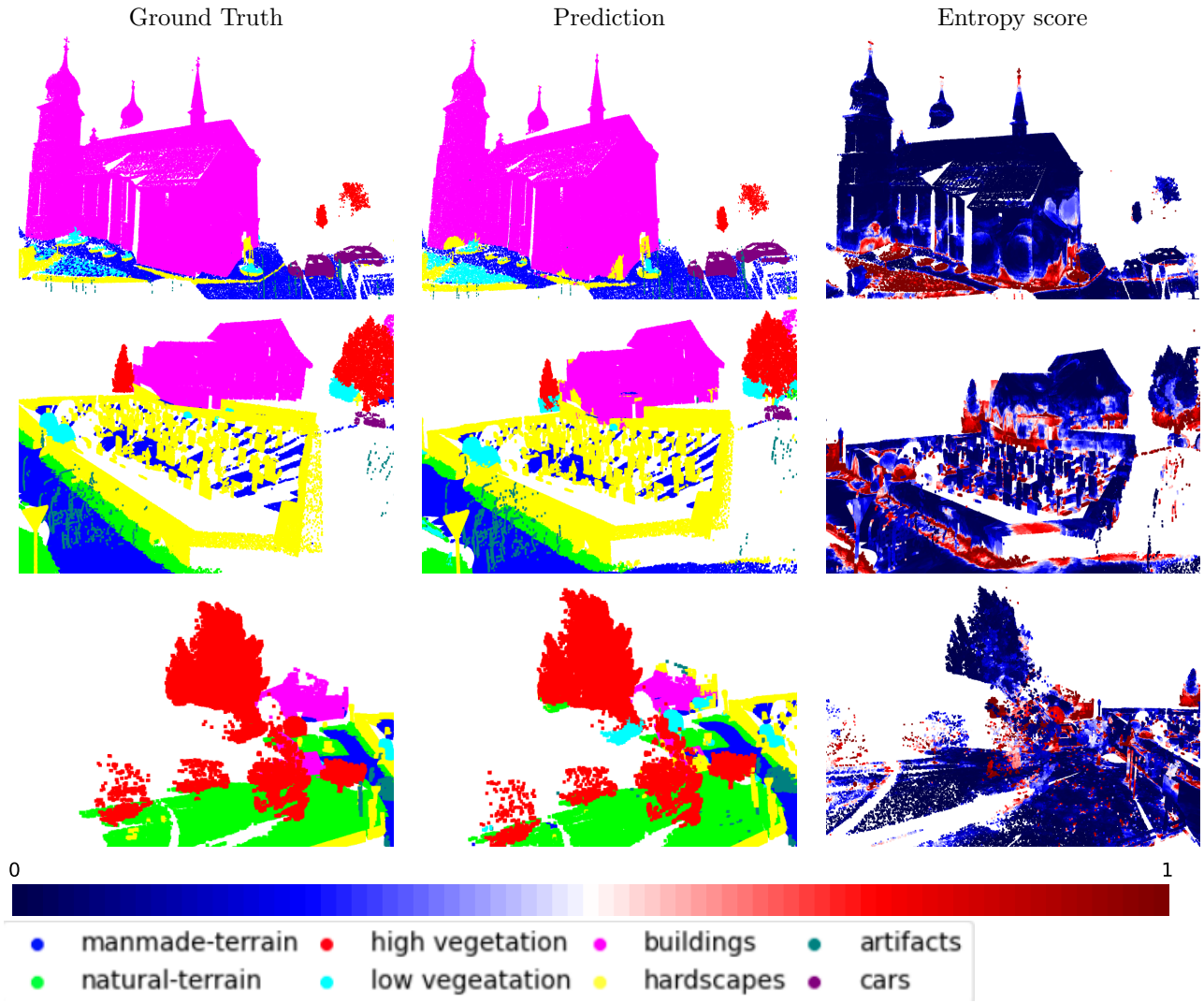

Figure 7.10: Perpoint entropy visualization of the semantic3D dataset.

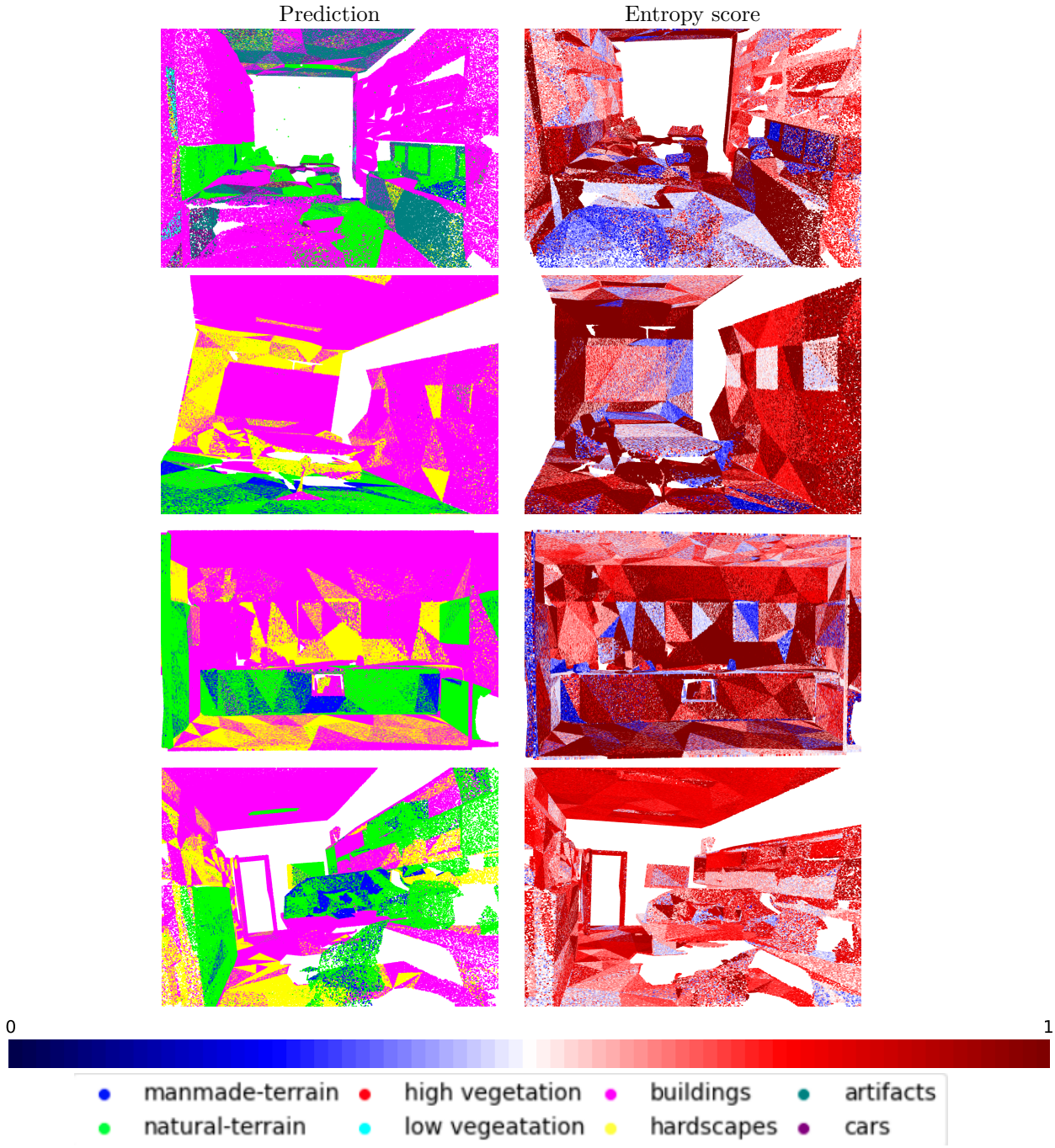

Figure 7.11: Perpoint entropy visualization of the S3DIS dataset.

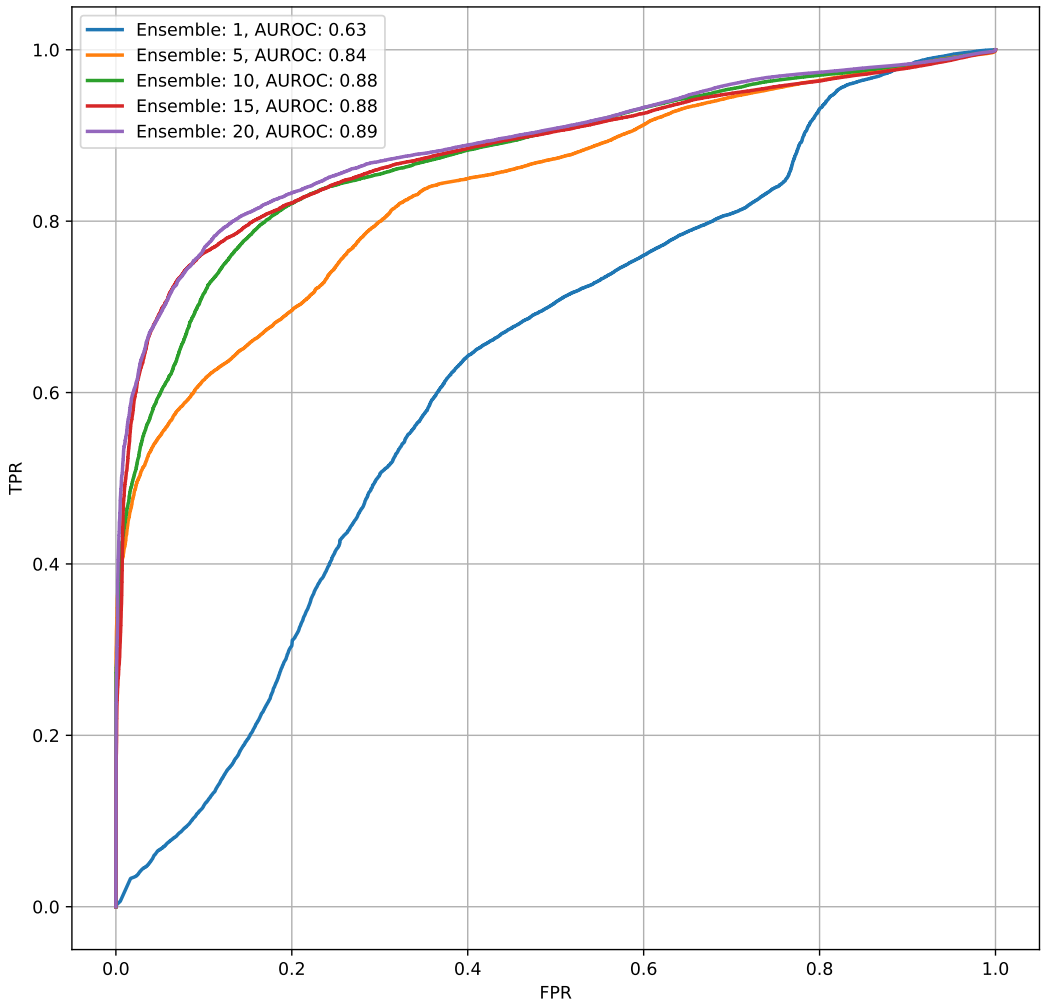

Figure 7.12: ROC plots and AUROC scores for entropy in semantic3D vs S3DIS

7.4 Flipout Vs Ensembles comparison

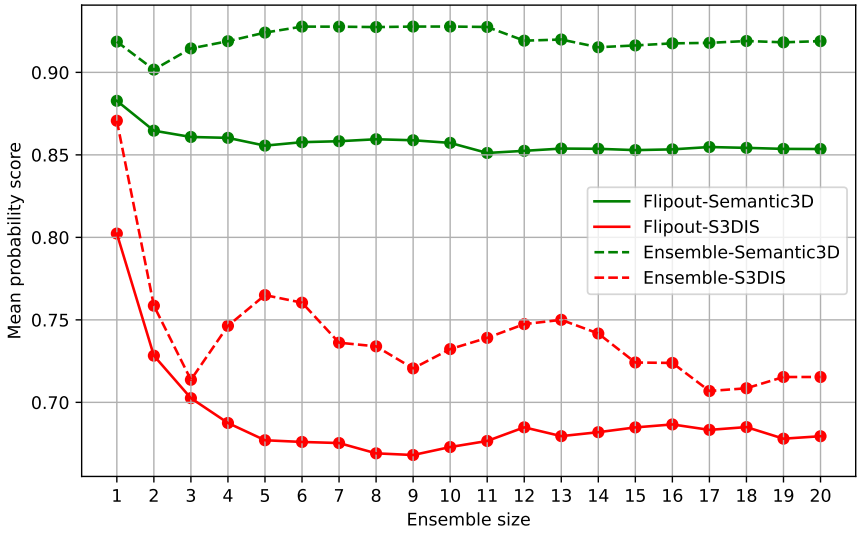

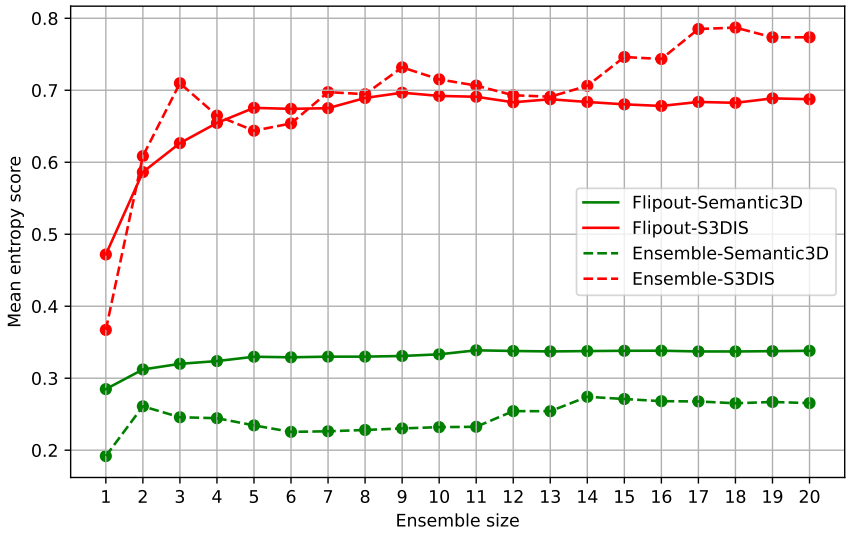

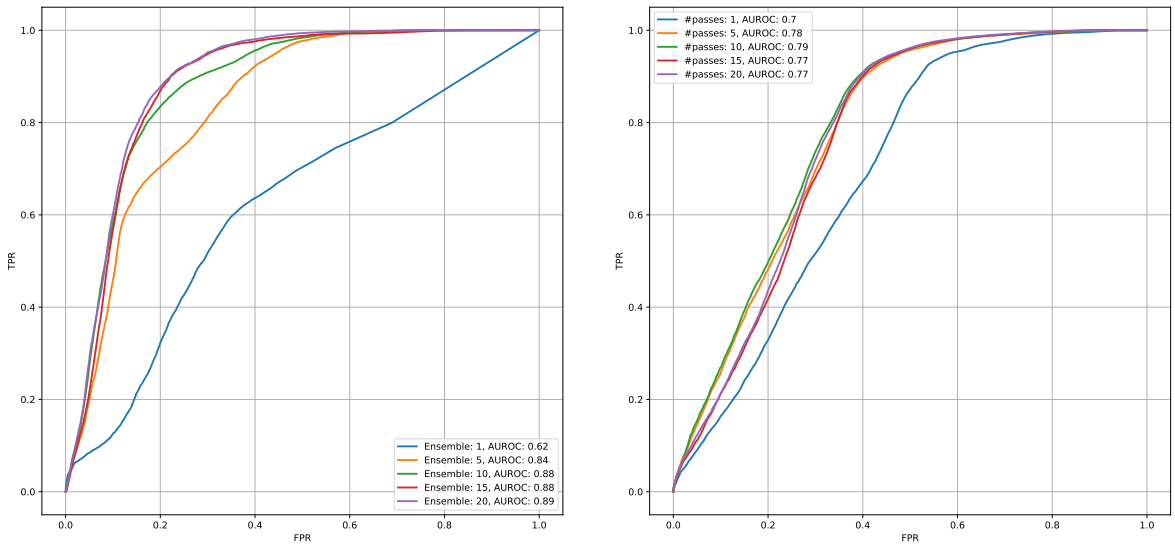

Figure 7.13: Ensmeble Vs Flipout - Probability scores

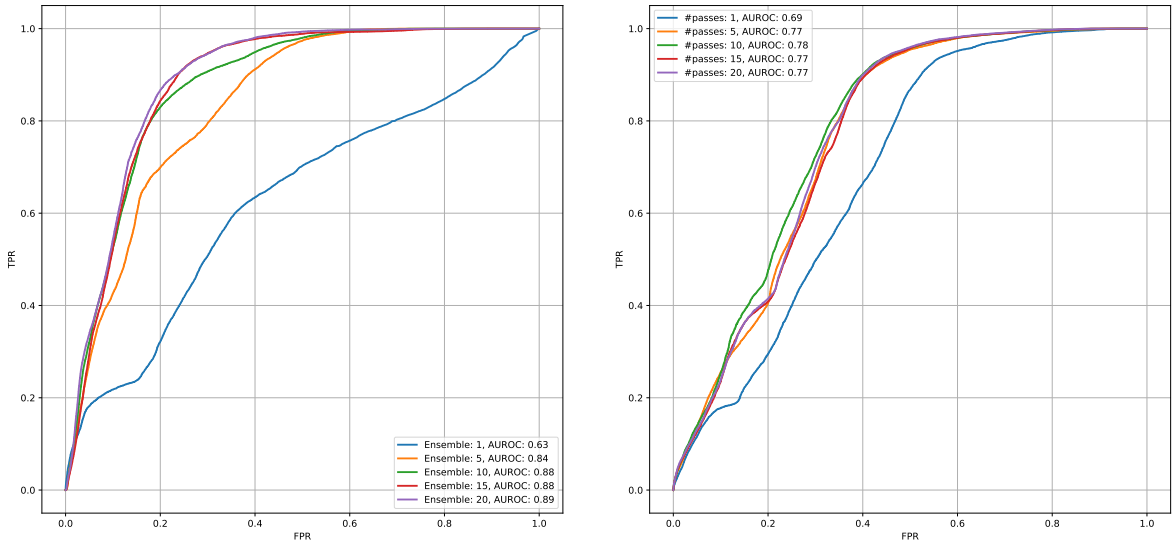

Figure 7.14: Ensemble Vs Flipout - Entropy scores

8

Conclusions

8.1 Contributions

8.2 Lessons learned

8.3 Future work

9

Notes/Remarks

A

DNN Safety

A.1 Safety of DNNs

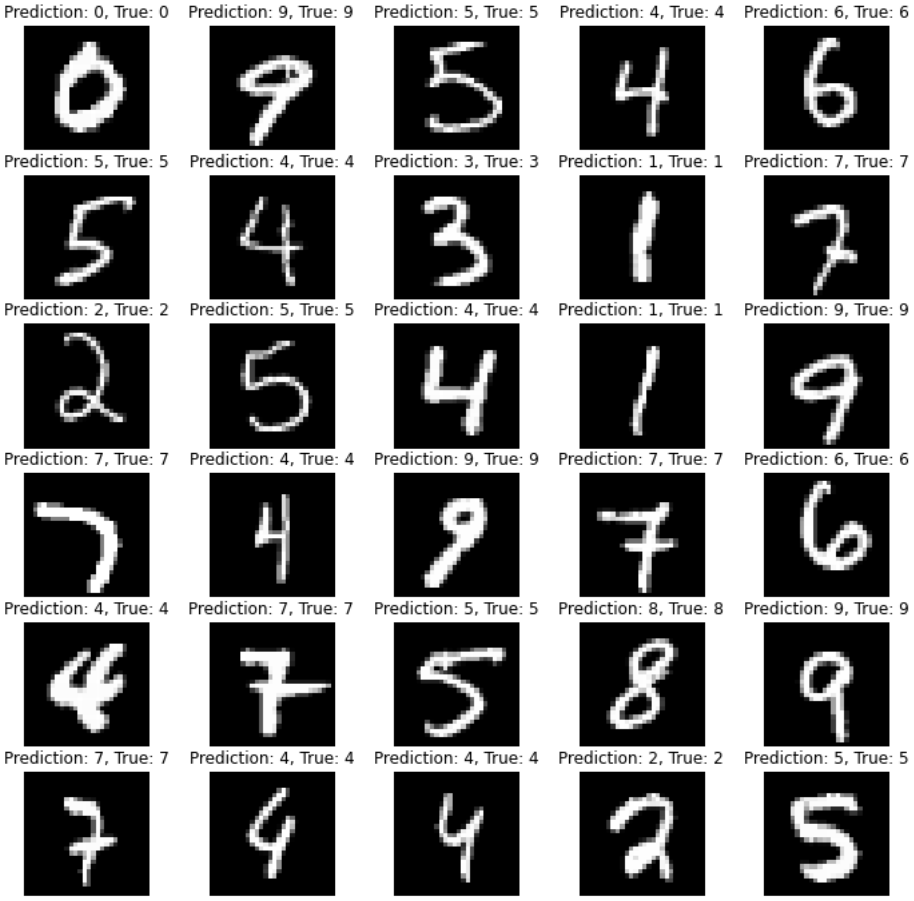
Prediction: 0, True: 0
Prediction: 9, True: 9
Prediction: 5, True: 5
Prediction: 4, True: 4
Prediction: 6, True: 6
Prediction: 5, True: 5
Prediction: 4, True: 4
Prediction: 3, True: 3
Prediction: 1, True: 1
Prediction: 7, True: 7
Prediction: 2, True: 2
Prediction: 5, True: 5
Prediction: 4, True: 4
Prediction: 1, True: 1
Prediction: 9, True: 9
Prediction: 7, True: 7
Prediction: 4, True: 4
Prediction: 9, True: 9
Prediction: 7, True: 7
Prediction: 6, True: 6
Prediction: 4, True: 4
Prediction: 7, True: 7
Prediction: 5, True: 5
Prediction: 8, True: 8
Prediction: 9, True: 9
Prediction: 7, True: 7
Prediction: 4, True: 4
Prediction: 4, True: 4
Prediction: 2, True: 2
Prediction: 5, True: 5

Figure A.1

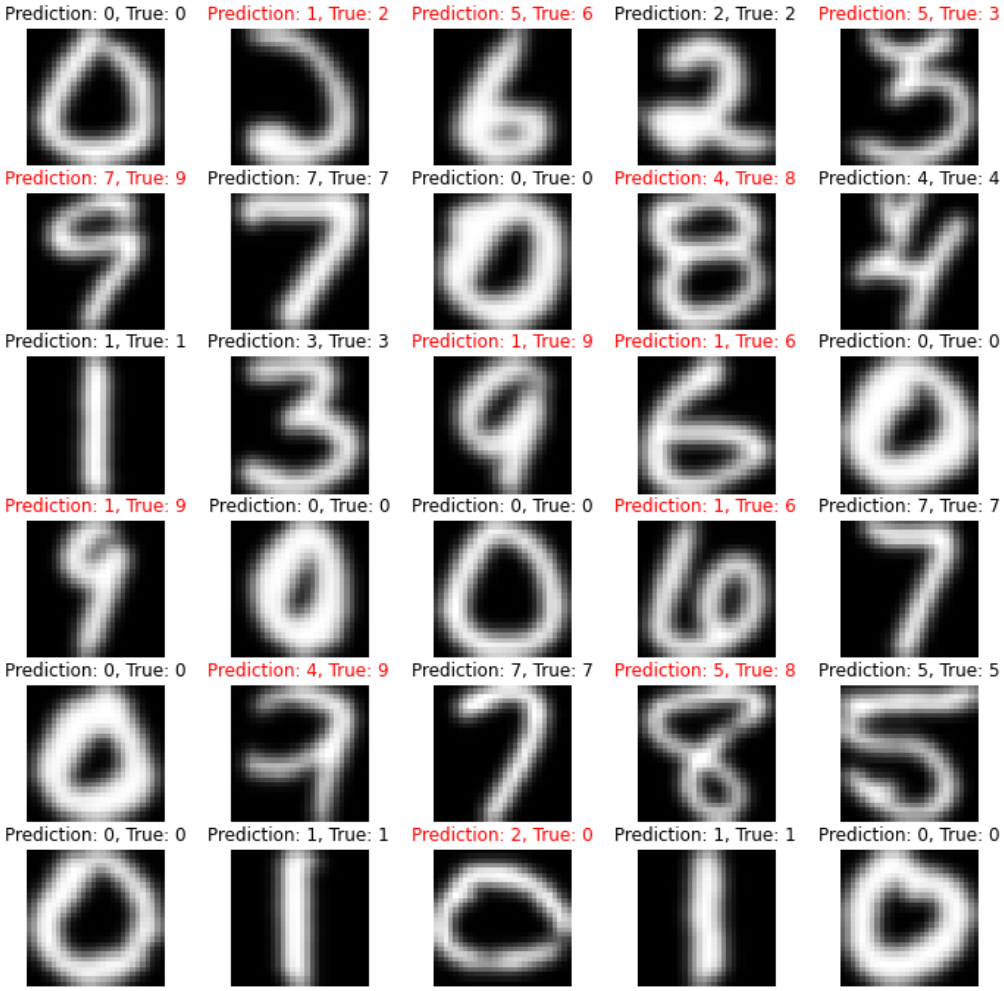
Prediction: 0, True: 0
Prediction: 1, True: 2
Prediction: 5, True: 6
Prediction: 2, True: 2
Prediction: 5, True: 3
Prediction: 7, True: 9
Prediction: 7, True: 7
Prediction: 0, True: 0
Prediction: 4, True: 8
Prediction: 4, True: 4
Prediction: 1, True: 1
Prediction: 3, True: 3
Prediction: 1, True: 9
Prediction: 1, True: 6
Prediction: 0, True: 0
Prediction: 1, True: 9
Prediction: 0, True: 0
Prediction: 0, True: 0
Prediction: 1, True: 6
Prediction: 7, True: 7
Prediction: 0, True: 0
Prediction: 4, True: 9
Prediction: 7, True: 7
Prediction: 5, True: 8
Prediction: 5, True: 5
Prediction: 0, True: 0
Prediction: 1, True: 1
Prediction: 2, True: 0
Prediction: 1, True: 1
Prediction: 0, True: 0

Figure A.2

B

Parameters

Your second chapter appendix

References

[1] Eren Erdal Aksoy, Saimir Baci, and Selcuk Cavdar. Salsanet: Fast road and vehicle segmentation in lidar point clouds for autonomous driving. In *IEEE Intelligent Vehicles Symposium (IV2020)*, 2020.

[2] Iñigo Alonso, Luis Riazuelo, Luis Montesano, and Ana C. Murillo. 3d-mininet: Learning a 2d representation from point clouds for fast and efficient 3d lidar semantic segmentation. *IEEE Robotics and Automation Letters*, 5(4):5432–5439, 2020. doi: 10.1109/LRA.2020.3007440.

[3] Iro Armeni, Ozan Sener, Amir R. Zamir, Helen Jiang, Ioannis Brilakis, Martin Fischer, and Silvio Savarese. 3d semantic parsing of large-scale indoor spaces. In *Proceedings of the IEEE Conference on Computer Vision and Pattern Recognition (CVPR)*, June 2016.

[4] Max Bajracharya, Mark W. Maimone, and Daniel Helmick. Autonomy for mars rovers: Past, present, and future. *Computer*, 41(12):44–50, 2008.

[5] Jens Behley, Martin Garbade, Andres Milioto, Jan Quenzel, Sven Behnke, Cyrill Stachniss, and Jurgen Gall. Semantickitti: A dataset for semantic scene understanding of lidar sequences. In *Proceedings of the IEEE/CVF International Conference on Computer Vision (ICCV)*, October 2019.

[6] Swaroop Bhandary K, Nico Hochgeschwender, Paul Plöger, Frank Kirchner, and Matias Valdenegro-Toro. Evaluating uncertainty estimation methods on 3d semantic segmentation of point clouds. *arXiv e-prints*, pages arXiv–2007, 2020.

[7] Bir Bhanu, Sungkee Lee, Chih-Cheng Ho, and Tom Henderson. Range data processing: Representation of surfaces by edges. In *Proceedings of the eighth international conference on pattern recognition*, pages 236–238. IEEE Computer Society Press, 1986.

[8] Holger Caesar, Varun Bankiti, Alex H Lang, Sourabh Vora, Venice Erin Liong, Qiang Xu, Anush Krishnan, Yu Pan, Giancarlo Baldan, and Oscar Beijbom. nuscenes: A multimodal dataset for autonomous driving. In *Proceedings of the IEEE/CVF conference on computer vision and pattern recognition*, pages 11621–11631, 2020.

[9] Varun Chandola, Arindam Banerjee, and Vipin Kumar. Anomaly detection: A survey. *ACM Comput. Surv.*, 41(3), july 2009. ISSN 0360-0300.

[10] Tiago Cortinhal, George Tzelepis, and Eren Erdal Aksoy. Salsanext: Fast, uncertainty-aware semantic segmentation of lidar point clouds. In George Bebis, Zhaozheng Yin, Edward Kim, Jan Bender, Kartic Subr, Bum Chul Kwon, Jian Zhao, Denis Kalkofen, and George Baciu, editors, *Advances in Visual Computing*, pages 207–222, Cham, 2020. Springer International Publishing. ISBN 978-3-030-64559-5.

[11] Mark De Deuge, Alastair Quadros, Calvin Hung, and Bertrand Douillard. Unsupervised feature learning for classification of outdoor 3d scans. In *Australasian Conference on Robitics and Automation*, volume 2, page 1, 2013.

[12] Haoyang Fan, Fan Zhu, Changchun Liu, Liangliang Zhang, Li Zhuang, Dong Li, Weicheng Zhu, Jiangtao Hu, Hongye Li, and Qi Kong. Baidu apollo em motion planner. *arXiv preprint arXiv:1807.08048*, 2018.

[13] Biao Gao, Yancheng Pan, Chengkun Li, Sibo Geng, and Huijing Zhao. Are we hungry for 3d lidar data for semantic segmentation? a survey of datasets and methods. *IEEE Transactions on Intelligent Transportation Systems*, pages 1–19, 2021. doi: 10.1109/TITS.2021.3076844.

[14] Candeo gauisus. Kursura as a museum ship in visakhapatnam, 2008. URL `https://en.wikipedia.org/wiki/INS_Kursura_(S20)#/media/File:INS_Kursura_(S20).jpg`. [Online; accessed December 20, 2021].

[15] Joachim Gehrung, Marcus Hebel, Michael Arens, and Uwe Stilla. An approach to extract moving objects from mls data using a volumetric background representation. *ISPRS Annals of Photogrammetry, Remote Sensing & Spatial Information Sciences*, 4, 2017.

[16] Jakob Geyer, Yohannes Kassahun, Mentar Mahmudi, Xavier Ricou, Rupesh Durgesh, Andrew S Chung, Lorenz Hauswald, Viet Hoang Pham, Maximilian Mühlegg, Sebastian Dorn, et al. A2d2: Audi autonomous driving dataset. *arXiv preprint arXiv:2004.06320*, 2020.

[17] Ross B. Girshick. Fast R-CNN. In *2015 IEEE International Conference on Computer Vision, ICCV 2015, Santiago, Chile, December 7-13, 2015*, pages 1440–1448. IEEE Computer Society, 2015.

[18] David Griffiths and Jan Boehm. Synthcity: A large scale synthetic point cloud. *arXiv preprint arXiv:1907.04758*, 2019.

[19] Timo Hackel, Nikolay Savinov, Lubor Ladicky, Jan D Wegner, Konrad Schindler, and Marc Pollefeys. Semantic3d. net: A new large-scale point cloud classification benchmark. *arXiv preprint arXiv:1704.03847*, 2017.

[20] Wolfgang Hess, Damon Kohler, Holger Rapp, and Daniel Andor. Real-time loop closure in 2d lidar slam. In *2016 IEEE International Conference on Robotics and Automation (ICRA)*, pages 1271–1278, 2016. doi: 10.1109/ICRA.2016.7487258.

[21] Dr. Karl-Heinz Hochhaus. Ms hamburg in plantours livery, 2013. URL `https://en.wikipedia.org/wiki/MS_Hamburg#/media/File:2013-05_11_Hamburg_DSCI2958_P.JPG`. [Online; accessed December 20, 2021].

[22] John Houston, Guido Zuidhof, Luca Bergamini, Yawei Ye, Long Chen, Ashesh Jain, Sammy Omari, Vladimir Iglovikov, and Peter Ondruska. One thousand and one hours: Self-driving motion prediction dataset. *arXiv preprint arXiv:2006.14480*, 2020.

[23] Qingyong Hu, Bo Yang, Linhai Xie, Stefano Rosa, Yulan Guo, Zhihua Wang, Niki Trigoni, and Andrew Markham. Randla-net: Efficient semantic segmentation of large-scale point clouds. In *Proceedings of the IEEE/CVF Conference on Computer Vision and Pattern Recognition (CVPR)*, June 2020.

[24] Deyvid Kochanov, Fatemeh Karimi Nejadasl, and Olaf Booij. Kprnet: Improving projection-based lidar semantic segmentation. *arXiv preprint arXiv:2007.12668*, 2020.

[25] K. Koster and M. Spann. Mir: an approach to robust clustering-application to range image segmentation. *IEEE Transactions on Pattern Analysis and Machine Intelligence*, 22(5):430–444, 2000. doi: 10.1109/34.857001.

[26] Alex Krizhevsky, Ilya Sutskever, and Geoffrey E. Hinton. Imagenet classification with deep convolutional neural networks. In Peter L. Bartlett, Fernando C. N. Pereira, Christopher J. C. Burges, Léon Bottou, and Kilian Q. Weinberger, editors, *Advances in Neural Information Processing Systems 25: 26th Annual Conference on Neural Information Processing Systems 2012. Proceedings of a meeting held December 3-6, 2012, Lake Tahoe, Nevada, United States*, pages 1106–1114, 2012.

[27] Balaji Lakshminarayanan, Alexander Pritzel, and Charles Blundell. Simple and scalable predictive uncertainty estimation using deep ensembles. *arXiv preprint arXiv:1612.01474*, 2016.

[28] Tim Levin. Tesla's full self-driving tech keeps getting fooled by the moon, billboards, and burger king signs, 2021. URL `https://www.businessinsider.in/thelife/news/teslas-full-self-driving-tech-keeps-getting-fooled-by-the-moon-billboards-and-burger-king-signs/articleshow/84769896.cms`. [Online; accessed December 24, 2021].

[29] Jesse Levinson, Jake Askeland, Jan Becker, Jennifer Dolson, David Held, Soeren Kammel, J. Zico Kolter, Dirk Langer, Oliver Pink, Vaughan Pratt, Michael Sokolsky, Ganymed Stanek, David Stavens, Alex Teichman, Moritz Werling, and Sebastian Thrun. Towards fully autonomous driving: Systems and algorithms. In *2011 IEEE Intelligent Vehicles Symposium (IV)*, pages 163–168, 2011.

[30] Bo Li, Tianlei Zhang, and Tian Xia. Vehicle detection from 3d lidar using fully convolutional network. *arXiv preprint arXiv:1608.07916*, 2016.

[31] M. Maurette. Mars rover autonomous navigation. *Autonomous Robots*, 14(2):199–208, Mar 2003. ISSN 1573-7527.

[32] Andres Milioto, Ignacio Vizzo, Jens Behley, and Cyrill Stachniss. Rangenet ++: Fast and accurate lidar semantic segmentation. In *2019 IEEE/RSJ International Conference on Intelligent Robots and Systems (IROS)*, pages 4213–4220, 2019. doi: 10.1109/IROS40897.2019.8967762.

[33] Laura A. Moore. Container ship mv maersk alabama leaves mombasa, kenya, 2009. URL `https://en.wikipedia.org/wiki/Container_ship#/media/File:Container_ship_MV_Maersk_Alabama.jpg`. [Online; accessed December 20, 2021].

[34] G. P. Moustris, S. C. Hiridis, K. M. Deliparaschos, and K. M. Konstantinidis. Evolution of autonomous and semi-autonomous robotic surgical systems: a review of the literature. *The International Journal of Medical Robotics and Computer Assisted Surgery*, 7(4):375–392, 2011.

[35] Daniel Munoz, J. Andrew Bagnell, Nicolas Vandapel, and Martial Hebert. Contextual classification with functional max-margin markov networks. In *2009 IEEE Conference on Computer Vision and Pattern Recognition*, pages 975–982, 2009. doi: 10.1109/CVPR.2009.5206590.

[36] Yancheng Pan, Biao Gao, Jilin Mei, Sibo Geng, Chengkun Li, and Huijing Zhao. Semanticposs: A point cloud dataset with large quantity of dynamic instances, 2020.

[37] Benjamin J Patz, Yiannis Papelis, Remo Pillat, Gary Stein, and Don Harper. A practical approach to robotic design for the darpa urban challenge. *Journal of Field Robotics*, 25(8):528–566, 2008.

[38] Charles R. Qi, Hao Su, Kaichun Mo, and Leonidas J. Guibas. Pointnet: Deep learning on point sets for 3d classification and segmentation. In *Proceedings of the IEEE Conference on Computer Vision and Pattern Recognition (CVPR)*, July 2017.

[39] Charles R Qi, Li Yi, Hao Su, and Leonidas J Guibas. Pointnet++: Deep hierarchical feature learning on point sets in a metric space. *arXiv preprint arXiv:1706.02413*, 2017.

[40] Shaoqing Ren, Kaiming He, Ross B. Girshick, and Jian Sun. Faster R-CNN: towards real-time object detection with region proposal networks. In Corinna Cortes, Neil D. Lawrence, Daniel D. Lee, Masashi Sugiyama, and Roman Garnett, editors, *Advances in Neural Information Processing Systems 28: Annual Conference on Neural Information Processing Systems 2015, December 7-12, 2015, Montreal, Quebec, Canada*, pages 91–99, 2015.

[41] Yuriy Reshetyuk. A unified approach to self-calibration of terrestrial laser scanners. *ISPRS Journal of Photogrammetry and Remote Sensing*, 65(5):445–456, 2010. ISSN 0924-2716.

[42] Radu Alexandru Rosu, Peer Schütt, Jan Quenzel, and Sven Behnke. Latticenet: Fast point cloud segmentation using permutohedral lattices. *arXiv preprint arXiv:1912.05905*, 2019.

[43] Xavier Roynard, Jean-Emmanuel Deschaud, and François Goulette. Paris-lille-3d: A large and high-quality ground-truth urban point cloud dataset for automatic segmentation and classification. *The International Journal of Robotics Research*, 37(6):545–557, 2018.

[44] Ruwen Schnabel, Roland Wahl, and Reinhard Klein. Efficient ransac for point-cloud shape detection. In *Computer graphics forum*, volume 26, pages 214–226. Wiley Online Library, 2007.

[45] Andrés Serna, Beatriz Marcotegui, François Goulette, and Jean-Emmanuel Deschaud. Paris-rue-Madame database: a 3D mobile laser scanner dataset for benchmarking urban detection, segmentation and classification methods. In *4th International Conference on Pattern Recognition, Applications and Methods ICPRAM 2014*, Angers, France, March 2014.

[46] Christian Spahrbier. Port anniversary-ship arrivals, 2019. URL `https://www.hamburg.com/port-anniversary/11615722/ship-arrivals/`. [Online; accessed December 20, 2021].

[47] Francis Godolphin Osbourne Stuart. The titanic departing southampton on april 10, 1912, 1912. URL `https://de.wikipedia.org/wiki/RMS_Titanic#/media/Datei:RMS_Titanic_3.jpg`. [Online; accessed December 20, 2021].

[48] Hang Su, Varun Jampani, Deqing Sun, Subhransu Maji, Evangelos Kalogerakis, Ming-Hsuan Yang, and Jan Kautz. Splatnet: Sparse lattice networks for point cloud processing. In *Proceedings of the IEEE Conference on Computer Vision and Pattern Recognition (CVPR)*, June 2018.

[49] Weikai Tan, Nannan Qin, Lingfei Ma, Ying Li, Jing Du, Guorong Cai, Ke Yang, and Jonathan Li. Toronto-3d: A large-scale mobile lidar dataset for semantic segmentation of urban roadways. In *Proceedings of the IEEE/CVF Conference on Computer Vision and Pattern Recognition Workshops*, pages 202–203, 2020.

[50] Haotian* Tang, Zhijian* Liu, Shengyu Zhao, Yujun Lin, Ji Lin, Hanrui Wang, and Song Han. Searching efficient 3d architectures with sparse point-voxel convolution. In *European Conference on Computer Vision*, 2020.

[51] Fayez Tarsha-Kurdi, Tania Landes, and Pierre Grussenmeyer. Hough-transform and extended ransac algorithms for automatic detection of 3d building roof planes from lidar data. In *ISPRS Workshop on Laser Scanning 2007 and SilviLaser 2007*, volume 36, pages 407–412, 2007.

[52] Maxim Tatarchenko, Jaesik Park, Vladlen Koltun, and Qian-Yi Zhou. Tangent convolutions for dense prediction in 3d. In *Proceedings of the IEEE Conference on Computer Vision and Pattern Recognition (CVPR)*, June 2018.

[53] Sebastian Thrun, Mike Montemerlo, Hendrik Dahlkamp, David Stavens, Andrei Aron, James Diebel, Philip Fong, John Gale, Morgan Halpenny, Gabriel Hoffmann, et al. Stanley: The robot that won the darpa grand challenge. *Journal of field Robotics*, 23(9):661–692, 2006.

[54] Weltrundschau zu Reclams Universum 1913 Unknown author. Lz 18 (l 2), 1913. URL `https://en.wikipedia.org/wiki/Zeppelin#/media/File:LZ_18.jpg`. [Online; accessed December 20, 2021].

[55] Mikaela Angelina Uy, Quang-Hieu Pham, Binh-Son Hua, Thanh Nguyen, and Sai-Kit Yeung. Revisiting point cloud classification: A new benchmark dataset and classification model on real-world data. In *Proceedings of the IEEE/CVF International Conference on Computer Vision (ICCV)*, October 2019.

[56] Bruno Vallet, Mathieu Brédif, Andrés Serna, Beatriz Marcotegui, and Nicolas Paparoditis. Terramobilita/iqmulus urban point cloud analysis benchmark. *Computers & Graphics*, 49:126–133, 2015. ISSN 0097-8493.

[57] Nina Varney, Vijayan K Asari, and Quinn Graehling. Dales: A large-scale aerial lidar data set for semantic segmentation. In *Proceedings of the IEEE/CVF Conference on Computer Vision and Pattern Recognition Workshops*, pages 186–187, 2020.

[58] George Vosselman, Sander Dijkman, et al. 3d building model reconstruction from point clouds and ground plans. *International archives of photogrammetry remote sensing and spatial information sciences*, 34(3/W4):37–44, 2001.

[59] Chengjia Wang, Tom MacGillivray, Gillian Macnaught, Guang Yang, and David Newby. A two-stage 3d unet framework for multi-class segmentation on full resolution image. *arXiv preprint arXiv:1804.04341*, 2018.

[60] Xinshuo Weng, Yunze Man, Dazhi Cheng, Jinhyung Park, Matthew O'Toole, and Kris Kitani. All-In-One Drive: A Large-Scale Comprehensive Perception Dataset with High-Density Long-Range Point Clouds. *arXiv*, 2020.

[61] Bichen Wu, Alvin Wan, Xiangyu Yue, and Kurt Keutzer. Squeezeseg: Convolutional neural nets with recurrent crf for real-time road-object segmentation from 3d lidar point cloud. In *2018 IEEE International Conference on Robotics and Automation (ICRA)*, pages 1887–1893, 2018. doi: 10.1109/ICRA.2018.8462926.

[62] Bichen Wu, Xuanyu Zhou, Sicheng Zhao, Xiangyu Yue, and Kurt Keutzer. Squeezesegv2: Improved model structure and unsupervised domain adaptation for road-object segmentation from a lidar point cloud. In *2019 International Conference on Robotics and Automation (ICRA)*, pages 4376–4382, 2019. doi: 10.1109/ICRA.2019.8793495.

[63] Pengchuan Xiao, Zhenlei Shao, Steven Hao, Zishuo Zhang, Xiaolin Chai, Judy Jiao, Zesong Li, Jian Wu, Kai Sun, Kun Jiang, Yunlong Wang, and Diange Yang. Pandaset: Advanced sensor suite dataset for autonomous driving. In *2021 IEEE International Intelligent Transportation Systems Conference (ITSC)*, pages 3095–3101, 2021. doi: 10.1109/ITSC48978.2021.9565009.

[64] Jun Xie, Martin Kiefel, Ming-Ting Sun, and Andreas Geiger. Semantic instance annotation of street scenes by 3d to 2d label transfer. In *Proceedings of the IEEE Conference on Computer Vision and Pattern Recognition (CVPR)*, June 2016.

[65] Chenfeng Xu, Bichen Wu, Zining Wang, Wei Zhan, Peter Vajda, Kurt Keutzer, and Masayoshi Tomizuka. Squeezesegv3: Spatially-adaptive convolution for efficient point-cloud segmentation. In *European Conference on Computer Vision*, pages 1–19. Springer, 2020.

[66] Bin Yang, Wenjie Luo, and Raquel Urtasun. Pixor: Real-time 3d object detection from point clouds. In *Proceedings of the IEEE Conference on Computer Vision and Pattern Recognition (CVPR)*, June 2018.

[67] Yang Zhang, Zixiang Zhou, Philip David, Xiangyu Yue, Zerong Xi, Boqing Gong, and Hassan Foroosh. Polarnet: An improved grid representation for online lidar point clouds semantic segmentation. In *Proceedings of the IEEE/CVF Conference on Computer Vision and Pattern Recognition (CVPR)*, June 2020.

[68] Yin Zhou and Oncel Tuzel. Voxelnet: End-to-end learning for point cloud based 3d object detection. In *Proceedings of the IEEE conference on computer vision and pattern recognition*, pages 4490–4499, 2018.

[69] Xinge Zhu, Hui Zhou, Tai Wang, Fangzhou Hong, Yuexin Ma, Wei Li, Hongsheng Li, and Dahua Lin. Cylindrical and asymmetrical 3d convolution networks for lidar segmentation. *arXiv preprint arXiv:2011.10033*, 2020.